energies

MDPI

*Article*

# Simulation-Based Resiliency Assessment of Hybrid Energy Systems: Application to a Sustainable Community in Africa

**Hossam A. Gabbar * and Zainab Lawal**

Faculty of Engineering and Applied Science, Ontario Tech University, Oshawa, ON L1G 0C5, Canada
* Correspondence: hossam.gabbar@ontariotechu.ca; Tel.: +1-9057218668 (ext. 5497)

**Abstract**

Reliable delivery of electricity, freshwater, hydrogen, and cooling remains challenging in remote communities where these services share generation, conversion, and storage resources. This study develops a simulation-based framework for assessing resiliency of multi-service performance under prescribed disturbances in Gbamu-Gbamu, Nigeria. The proposed multigeneration system combines renewable and waste-to-energy/biogas resources with battery and hydrogen storage, fuel-cell support, desalination, and cooling. MG-OPT, implemented in Python 3.13.18 and executed in Google Colab, MATLAB R2026a Update 5 with Simulink 26.1 (R2026a), and HOMER Pro 3.18.3 (64-bit, Pro Edition) support configuration assessment, technology comparisons, disturbance simulations, and techno-economic analysis. Individual service-coverage indicators and an Integrated Service Performance Score (ISPS) quantify demand satisfaction. Critical-service thresholds are assessed separately, while an eight-state descriptive framework defines operating conditions and response phases. Conditional fault-tree screening, dependence sensitivity tests, and Monte Carlo parameter propagation examine the effects of assumed event probabilities and selected dependencies. Four operating configurations are simulated. The Maximum Cooling Coverage case is selected for detailed assessment of a compound disturbance from 4.001 to 8.001 h. Its mean disturbance-period ISPS is 0.3188, and the Disturbance-Period Performance Preservation Index (DPPI) is 0.5249. Battery discharge and fuel-cell generation supply 232.75 and 31.81 kWh, respectively, over the 12 h simulation. However, aggregate village electricity supply remains below the 2.0833 kW critical-load proxy for 1.6443 h. Numerical checks support consistency with the implemented power balances, storage balances, and operating bounds. The assessment quantifies service degradation and its duration under prescribed availability signals without predicting physically calibrated equipment recovery. The findings identify service shortfalls and limitations of backup support, providing a basis for comparing operating configurations and dispatch settings.

**Keywords:** multigeneration energy system; hybrid energy systems; disturbance-response assessment; service coverage; performance preservation; fault tree analysis; Monte Carlo parameter propagation; hydrogen energy storage; waste-to-energy; techno-economic analysis

Check for updates

Academic Editor: Yang Du

Received: 26 September 2026
Revised: 12 November 2026
Accepted: 17 November 2026
Published: 26 November 2026

**Copyright:** © 2026 by the authors. Licensee MDPI, Basel, Switzerland. This article is an open access article distributed under the terms and conditions of the Creative Commons Attribution (CC BY) license.

## 1. Introduction

Climate change, energy-security concerns, and rising demand have accelerated the deployment of renewable energy technologies [1,2]. However, variable renewable generation creates supply challenges for remote and underserved communities. These challenges become more complex when electricity, freshwater, hydrogen, and cooling depend on shared

resources. Integrated hybrid multigeneration systems combine generation, storage, and conversion technologies to supply these interconnected services [3–5].

### 1.1. Background on Multigeneration Energy Systems

Multigeneration systems coordinate generation, conversion, and storage technologies to provide several services. Photovoltaic, wind, and geothermal resources can be combined with batteries, hydrogen technologies, desalination, and cooling [3–7]. These configurations can improve resource utilization and help meet electricity, freshwater, hydrogen, and cooling requirements. Multigeneration systems are particularly relevant to rural African communities, where substantial renewable-energy potential coexists with limited access to essential services and energy-storage infrastructure [1,2,8].

Studies on desalination illustrate the importance of process integration and energy use. Ahmed et al. [9] reviewed hybrid desalination technologies, highlighting their potential to reduce energy consumption compared with standalone processes. Ghaffour et al. [10] examined renewable-energy-driven desalination, emphasizing the importance of matching energy sources with suitable desalination technologies.

Previous studies have demonstrated the technical feasibility of renewable multigeneration systems under different climatic conditions and operating requirements [3–7]. Integrating service pathways can improve resource utilization, but it also creates dependencies. Hydrogen production and water treatment require electricity, while thermal resources can support desalination and cooling. A disturbance affecting shared generation, storage, or conversion equipment may therefore disrupt several services. Coordinating these interconnected pathways is an important modelling consideration. O'Dwyer et al. [11] integrated an energy management tool with a digital-twin testing environment to support the coordination and control of multi-vector energy systems.

High efficiency and demand satisfaction during normal operation do not establish how a system will perform during a disruption. Assessment must also consider service shortfalls, disturbance propagation, storage utilization, and critical-service availability. This study examines these consequences through time-dependent simulations under prescribed availability signals. Conditional probabilistic screening separately examines the effects of assumed event probabilities and selected dependencies.

### 1.2. Service Performance and Disturbance-Response Assessment

Reliability describes a system's ability to provide the required service under specified conditions over a defined period. Resilience concerns its ability to withstand, adapt to, and recover from disruptive events [12,13]. In multigeneration systems, shared resources create dependencies among services. Component failures, resource shortages, demand variations, and prolonged reductions in renewable generation can therefore affect several services simultaneously [8,12].

The resilience literature examines system performance throughout a disruption rather than considering demand satisfaction alone [14–16]. Common indicators include maximum performance loss, unmet demand, degradation duration, and cumulative performance loss. Recovery time and recovery rate are also relevant when supported by the model or observations. Probabilistic methods can examine event occurrence and restoration processes when suitable models and data are available. Individual service indicators remain necessary because aggregate performance can conceal service-specific shortfalls.

The present study evaluates electricity, freshwater, hydrogen production, and cooling in a rural Nigerian multigeneration system. Service-coverage indicators compare each output with its planning requirement. The Integrated Service Performance Score (ISPS)

combines these indicators into an aggregate measure of service adequacy. Critical-service thresholds and stored hydrogen reserves are assessed separately.

The Disturbance-Period Performance Preservation Index (DPPI), defined in Equation (16), expresses average ISPS during the prescribed disturbance window relative to its pre-disturbance reference. Equipment availability is prescribed over this interval. DPPI therefore measures performance preservation under the imposed conditions without representing an independently modelled physical recovery process. The eight-state descriptive framework classifies operating conditions and response phases when the required service indicators and operational-action records are available.

MG-OPT, HOMER, and MATLAB/Simulink support technology comparisons, feasibility assessment, disturbance simulations, and lifecycle economic analysis. The simulations track service delivery, storage utilization, and shortfalls relative to an aggregate critical electrical-load proxy. Fault tree analysis (FTA), dependence sensitivity tests, and Monte Carlo parameter propagation provide complementary screening under assumed event probabilities. Any return to baseline service coverage following scheduled input restoration is distinguished from physical equipment repair, restart, and replenishment of stored reserves.

### *1.3. Energy Access and Multi-Service Challenges in Africa*

Access to reliable energy, clean water, and other essential services remains a major challenge across Africa despite its substantial renewable-energy potential [1,2]. According to the International Energy Agency (IEA), approximately 600 million people in sub-Saharan Africa lacked electricity access in 2024, representing 47% of the region's population [17]. The World Bank also identified high electricity costs and unreliable supply as major challenges in West Africa [18]. Rural communities face geographic isolation, limited infrastructure, financing constraints, and high grid-expansion costs. Population growth, agricultural activity, and climate-related pressures further increase the need for decentralized service provision.

Rural hybrid energy systems are exposed to resource variability, extreme weather, component failures, storage depletion, and changing demand. In multigeneration configurations, shared generation, conversion, and storage resources can transmit the effects of these conditions across several services. Unreliable electricity also has substantial economic consequences. In 2023, the World Bank reported estimated annual losses of NGN 7–10 trillion in Nigeria, equivalent to approximately 5–7% of national GDP [19].

Hybrid renewable-energy systems and mini-grids have been investigated as ways to improve energy access and support rural development [1,20]. Research on Africa's water–energy–food nexus also emphasizes integrated resource planning [21,22]. However, component sizing and steady-state calculations alone do not establish the duration of service shortfalls during a disturbance. Assessing critical-service availability and depletion of shared storage reserves also requires examination of operating conditions over time.

This study applies the proposed framework to Gbamu-Gbamu, Nigeria, to examine interconnected electricity, freshwater, hydrogen-production, and cooling services. Four representative operating configurations are simulated, with one selected for detailed compound-disturbance assessment. The analysis quantifies service shortfalls and their duration under prescribed availability constraints while tracking storage utilization and critical electrical-service adequacy.

## 2. Hybrid Multigeneration System and Disturbance-Response Framework

This section describes the proposed hybrid multigeneration system and the framework used to assess its response to prescribed disturbances. The architecture connects generation, conversion, and storage technologies with electricity, freshwater, hydrogen-production, and cooling services. The assessment evaluates individual service coverage, aggregate

performance, and critical-service adequacy. Conditional probabilistic screening separately examines the effects of assumed event probabilities and selected dependencies.

### *2.1. Multigeneration Hybrid Energy System Design Framework*

The proposed system integrates renewable generation, energy conversion, storage, and energy management to support four interconnected community services: electricity, freshwater, hydrogen, and cooling. Figure 1 illustrates the principal resources, technologies, storage subsystems, and service pathways.

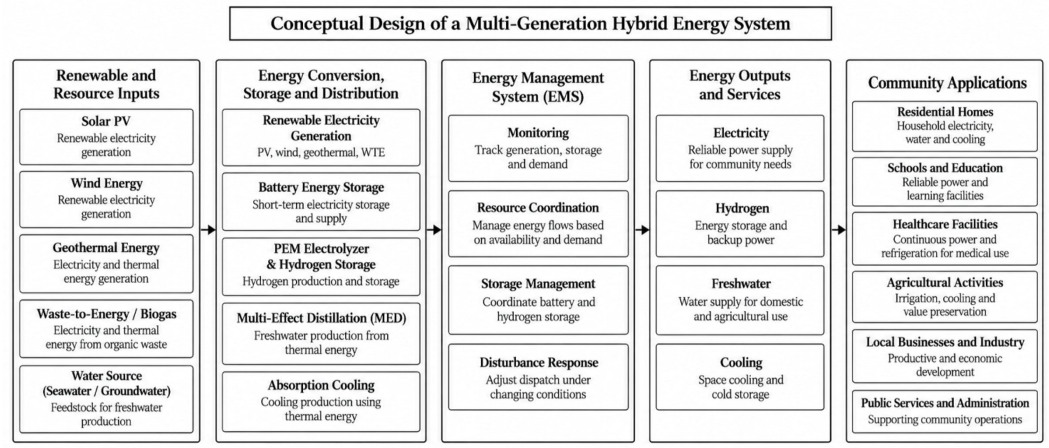


**Figure 1.** Conceptual architecture of the proposed hybrid multigeneration energy system.

Photovoltaic (PV), wind, geothermal, and waste-to-energy (WTE)/biogas pathways provide electricity, while battery storage supports short-term electrical balancing. A proton exchange membrane (PEM) electrolyzer produces hydrogen for storage and subsequent electricity generation through a fuel cell. In the reference architecture, thermal resources and recovered heat support freshwater production through multi-effect distillation (MED) and cooling through absorption refrigeration. The disturbance simulations represent freshwater and cooling provision through simplified power-allocation relationships, as described in the subsequent modelling sections.

Shared generation, conversion, and storage resources create dependencies among the four services. Changes in resource availability can affect service production, storage utilization, and backup generation. Hydrogen production and stored hydrogen inventory are tracked separately because previously stored hydrogen may remain available for fuel-cell operation when production decreases.

The energy management system (EMS) coordinates dispatch according to generation availability, storage conditions, service demand, and operating constraints. During electrical deficits, battery dispatch provides support within its power and state-of-charge limits. Fuel-cell output supplies additional support when requested, subject to rated power and accessible hydrogen inventory. The resulting trajectories show how dispatch and resource constraints affect service delivery over time.

MATLAB/Simulink integrates the generation, conversion, storage, and control representations within a common simulation environment. This environment supports model-based assessment under specified operating conditions. Continuous bidirectional synchronization with an operating physical system is outside the study's scope.

### *2.2. Multi-Service Performance and Disturbance-Response Assessment*

The framework evaluates service adequacy at each simulation time step and tracks performance during prescribed disturbances. Electricity, freshwater, hydrogen production,

and cooling are assessed individually using service-coverage indicators. The Integrated Service Performance Score (ISPS) combines these indicators into an aggregate measure. Critical-service requirements are evaluated separately against their specified thresholds. Figure 2 summarizes the assessment process.

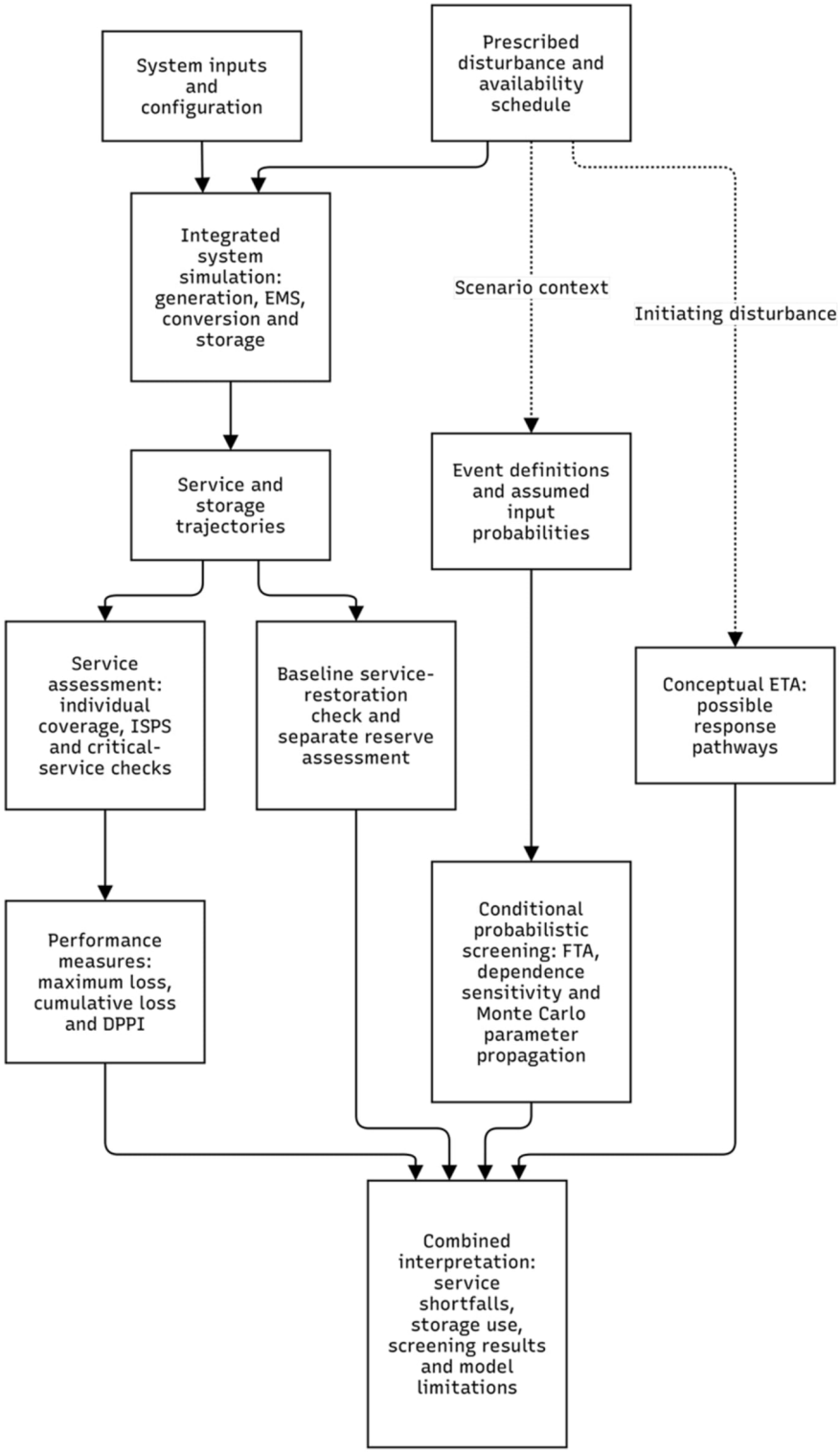


**Figure 2.** Multi-service performance and disturbance-response assessment framework for the proposed hybrid energy system.

Subsystem outputs determine the proportion of each service demand that is satisfied. Individual coverage indicators identify service-specific shortfalls, while ISPS summarizes aggregate service adequacy. Critical-service indicators and storage assessments provide additional information on essential requirements and available reserves. Hydrogen-production coverage is distinguished from stored hydrogen availability.

The simulated trajectories describe changes in service coverage and storage utilization over time. Maximum performance loss measures the greatest reduction relative to the pre-disturbance reference. Cumulative performance loss integrates the difference between reference and simulated performance over the specified interval. The Disturbance-Period Performance Preservation Index (DPPI) expresses average ISPS during the prescribed disturbance window relative to its pre-disturbance reference.

Return to baseline service coverage is confirmed only when the specified threshold and persistence requirements are satisfied. Restoration of subsystem availability is prescribed as a simulation input and does not itself establish service restoration. Physical equipment repair and restart dynamics are outside the model's scope, while storage replenishment is assessed separately.

The eight-state descriptive framework classifies operating conditions and response phases when the required service, reserve, and operational-action information is available. Emergency actions, repair activities, and confirmed recovery status require explicit supporting evidence. Conditional fault-tree screening, dependence sensitivity tests, and Monte Carlo parameter propagation separately examine how assumed probabilities and selected dependencies affect screening outcomes.

### *2.3. Proposed Multi-Service Assessment Framework*

This section presents the reference subsystem conversion relationships, service-performance indicators, and storage balances used in the assessment. The disturbance simulations use simplified power-allocation and stock–flow models to calculate service delivery and changes in storage over time. Conditional probabilistic screening separately evaluates event combinations under stated probability assumptions.

#### 2.3.1. Hydrogen Production

The proton exchange membrane (PEM) electrolyzer uses electricity from the integrated generation system to produce hydrogen. Hydrogen-production coverage compares the production rate with the specified community requirement. Stored hydrogen inventory is tracked separately to determine the reserve available for fuel-cell operation. Equation (1) gives the reference relationship between stack current and hydrogen production rate based on Faraday's law and Faradaic efficiency [23]. The factor of 2 accounts for the two electrons required to produce one hydrogen molecule, while the factor of 3600 converts the calculated production rate from kg/s to kg/h.

$$\dot{m}_{H_2} = \eta_F \frac{N_{\text{cell}} I M_{H_2}}{2F} \times 3600 \quad (1)$$

where

- $\dot{m}_{H_2}$ = hydrogen production rate (kg/h);
- $\eta_F$ = Faradaic efficiency of the PEM electrolyzer (dimensionless);
- $N_{\text{cell}}$ = number of electrolyzer cells;
- $I$ = current through each cell in the represented electrolyzer stack (A);
- $M_{H_2}$ = molar mass of hydrogen (kg/mol); and
- $F$ = Faraday's constant (96,485 C/mol).

Modelling assumptions: The disturbance simulations represent PEM electrolysis at the system level. Equation (1) provides the reference electrochemical relationship, with Faradaic

efficiency accounting for the fraction of current contributing to hydrogen formation. In the disturbance simulations, hydrogen production is calculated by dividing the electrical power allocated to the electrolyzer by its assumed specific electricity consumption. Allocated power is constrained by electrical availability, electrolyzer capacity, and the imposed availability signal. Section 4 specifies the conversion factor used. Electrolyzer start-up and shutdown transients, detailed cell-level dynamics, and temperature-dependent degradation are outside the model's scope.

#### 2.3.2. SOFC Electrical Power

The reference architecture includes a solid oxide fuel cell (SOFC) that uses stored hydrogen to supply backup electricity. Equation (2) relates the SOFC stack operating conditions to its electrical output after inverter conversion [5]. Inverter efficiency accounts for conversion losses, while division by 1000 converts watts to kilowatts.

$$P_{\mathrm{SOFC}} = \frac{N_{\mathrm{cell}} V_{\mathrm{cell}} I \eta_{\mathrm{inv}}}{1000} \tag{2}$$

where

- $P_{\mathrm{SOFC}}$ = SOFC electrical output after inverter conversion (kW);
- $N_{\mathrm{cell}}$ = number of cells in the SOFC stack;
- $V_{\mathrm{cell}}$ = operating cell voltage (V);
- $I$ = stack current (A); and
- $\eta_{\mathrm{inv}}$ = inverter efficiency (dimensionless).

Modelling assumptions: The disturbance simulations represent fuel-cell generation through an aggregate electrical conversion model. The fuel cell supplies the remaining power request after battery support, subject to rated power, imposed availability, and accessible hydrogen inventory. Hydrogen consumption is calculated from the dispatched electrical output using the assumed electrical energy yield per kilogram of hydrogen specified in Section 4. This yield is defined at the modelled electrical output boundary. Detailed polarization behaviour, thermal dynamics, degradation, and start-up and shutdown transients are outside the model's scope.

#### 2.3.3. SOFC Hydrogen Consumption

The SOFC draws hydrogen from storage to supply backup electricity. Increasing its electrical output can reduce service shortfalls but also reduces the hydrogen reserve available for later operation. Equation (3) relates electrical output to hydrogen consumption rate. Electrical output is defined after inverter conversion, and the effective conversion efficiency includes inverter losses to maintain a consistent output boundary.

$$\dot{m}_{H_2,\mathrm{SOFC}} = \frac{P_{\mathrm{SOFC}}}{\eta_{\mathrm{SOFC}} LHV_{H_2}} \tag{3}$$

where

- $\dot{m}_{H_2,\mathrm{SOFC}}$ = hydrogen-consumption rate (kg/h);
- $P_{\mathrm{SOFC}}$ = SOFC electrical output at the specified delivery boundary (kW);
- $\eta_{\mathrm{SOFC}}$ = effective electrical conversion efficiency at the same output boundary (dimensionless); and
- $LHV_{H_2}$ = lower heating value of hydrogen (kWh/kg).

Modelling assumptions: The disturbance simulations calculate hydrogen consumption by dividing dispatched fuel-cell power by the assumed electrical energy yield per kilogram of hydrogen. Section 4 specifies this yield at the modelled electrical output boundary. Fuel-cell dispatch and hydrogen withdrawal are constrained by rated power, imposed

availability, and accessible hydrogen inventory. Multiplying the consumption rate in kg/h by 24 expresses the equivalent rate in kg/day. Actual consumption over an interval is determined by integrating the rate over time. The model represents fuel-cell conversion at the system level. Detailed fuel processing, thermal dynamics, and transient electrochemical behaviour are outside its scope.

#### 2.3.4. Freshwater Production

The reference architecture includes a multi-effect distillation (MED) subsystem supplied with thermal energy from the integrated generation system [24]. Equation (4) defines the gained output ratio (GOR) as the ratio of freshwater production rate to heating-steam mass-flow rate [3,5]. Both rates are expressed in kg/h. When freshwater demand is expressed volumetrically, production is converted to matching units before service coverage is calculated.

$$GOR = \frac{\dot{m}_{fw}}{\dot{m}_{s}} \quad (4)$$

where

- $GOR$ = gained output ratio (dimensionless);
- $\dot{m}_{fw}$ = freshwater-production rate (kg/h); and
- $\dot{m}_{s}$ = heating-steam mass-flow rate (kg/h).

Modelling assumptions: Equation (4) represents MED performance using an aggregate GOR. Determining the available heating-steam supply requires a separate thermal-energy balance. In the disturbance simulations, freshwater production is calculated by dividing the allocated electrical power by the assumed specific electricity consumption specified in Section 4. This simplified relationship evaluates freshwater provision under electrical constraints. It does not resolve MED stage temperatures, pressures, salinity, or heat-transfer dynamics.

#### 2.3.5. Cooling Performance

The reference architecture includes an absorption chiller supplied with heat from the integrated system. Equation (5) relates useful cooling output to the heat supplied to the chiller generator through the thermal coefficient of performance (COP). Cooling-service coverage compares useful cooling output with cooling demand. MED and absorption cooling can draw on shared thermal resources, so allocating limited heat to one subsystem can reduce the heat available to the other.

$$Q_{cool} = COP \times Q_{gen} \quad (5)$$

where

- $COP$ = thermal coefficient of performance (dimensionless);
- $Q_{cool}$ = useful cooling output (kW); and
- $Q_{gen}$ = heat input to the absorption-chiller generator (kW).

Modelling assumptions: Equation (5) represents absorption cooling using an aggregate thermal COP. In the disturbance simulations, cooling output is calculated from allocated electrical-equivalent power using the conversion factor specified in Section 4. This factor is distinct from the thermal COP, which relates cooling output to heat input. The simplified representation evaluates cooling provision under electrical constraints and does not resolve competition for shared heat. Temperature-dependent and transient behaviour of the generator, absorber, condenser, and evaporator is outside its scope.

2.3.6. Service Coverage

Service coverage measures the fraction of demand met at a given time for electricity, freshwater, hydrogen production, and cooling. Individual indicators identify service-specific shortfalls before aggregation into an overall performance score. Their trajectories show how service adequacy changes during a disturbance. Hydrogen-production coverage is evaluated separately from stored hydrogen inventory, which determines the reserve available for fuel-cell operation.

$$C_i(t) = \min\left(1, \frac{S_i(t)}{D_i(t)}\right),\ i \in \{E, W, H, C\} \tag{6}$$

where

- $C_i(t)$ = coverage of service $i$ at time $t$ (dimensionless);
- $S_i(t)$ = supply or production rate of service $i$ at time $t$
- $D_i(t)$ = demand for service $i$ at time $t$; and
- $t$ = simulation time

The indices E, W, H, and C denote electricity, freshwater, hydrogen production, and cooling, respectively. Equation (6) caps each coverage indicator at one. A value of one indicates full satisfaction of the specified demand, while a lower value indicates a shortfall. Excess supply does not increase coverage beyond one.

Modelling assumptions: Supply and demand use consistent units for each service. The calculation assumes nonnegative supply and positive demand throughout the assessment interval. Hydrogen-production coverage compares production with the specified requirement. It does not establish delivery to end users or quantify stored hydrogen availability.

2.3.7. Integrated Service Performance Score (ISPS)

The Integrated Service Performance Score (ISPS) combines the four service-coverage indicators into a weighted measure of aggregate service adequacy at each simulation time step. Its trajectory provides the basis for calculating performance loss and performance preservation during prescribed disturbances.

$$ISPS(t) = \sum_{i \in \{E,W,H,C\}} w_i C_i(t) \tag{7}$$

$$\sum_{i \in \{E,W,H,C\}} w_i = 1,\ \ w_i \geq 0 \tag{8}$$

where

- $ISPS(t)$ = Integrated Service Performance Score at time $t$ (dimensionless);
- $C_i(t)$ = coverage of service $i$ at time $t$ (dimensionless);
- $w_i$ = weighting factor assigned to service $i$ (dimensionless);
- $i \in \{E,W,H,C\}$ identifies electricity, freshwater, hydrogen production, and cooling, respectively.

Equation (7) calculates ISPS as a weighted sum of the service-coverage indicators. Equation (8) requires nonnegative weights that sum to one. ISPS therefore ranges from zero to one, with higher values indicating greater aggregate service adequacy. Individual coverage indicators and critical-service assessments are reported alongside ISPS because the aggregate score can conceal a shortfall in a particular service.

Modelling assumptions: Equal weights of 0.25 are adopted as the reference scheme because stakeholder-derived priorities are unavailable. Each normalized coverage indicator therefore has the same influence on ISPS. This choice does not establish equal social or operational importance and is separate from EMS dispatch priorities. Alternative weights may be examined through sensitivity analysis. ISPS is calculated solely from service coverage and the assigned weights, without additional multipliers based on descriptive operating states.

2.3.8. Critical-Service Coverage

Critical-service coverage is evaluated separately from overall service coverage and ISPS. Equation (9) compares the supply delivered or explicitly allocated to critical users with the minimum requirement for the corresponding service. Coverage is capped at one, indicating full satisfaction of that requirement. A lower value indicates a shortfall.

$$C_{i,\mathrm{crit}}(t) = \min\left(1, \frac{S_{i,\mathrm{crit}}(t)}{D_{i,\mathrm{crit}}(t)}\right) \tag{9}$$

where:

- $C_{i,\mathrm{crit}}(t)$ = critical-service coverage for service $i$ at time $t$ (dimensionless);
- $S_{i,\mathrm{crit}}(t)$ = supply delivered or explicitly allocated to critical users of service $i$ at time $t$
- $D_{i,\mathrm{crit}}(t)$ = minimum critical-service requirement for service $i$ at time $t$.

Modelling assumptions: Critical-service thresholds are prescribed assessment criteria and are reported separately from normal service demand. Supply and the corresponding requirement are expressed in consistent units. Supply is assumed to be nonnegative, and the requirement must be positive. The disturbance simulations compare total village electricity served with a critical electrical-load threshold as an aggregate adequacy proxy. Supply below this threshold indicates an aggregate shortfall. Meeting or exceeding the threshold does not confirm delivery to individual critical facilities, which requires explicit allocation information. Hydrogen-reserve adequacy is assessed separately by comparing actual stored hydrogen mass with the specified reserve requirement, both expressed in kilograms.

2.3.9. Fault Tree Analysis—Conditional Probabilistic Screening

Fault tree analysis (FTA) represents combinations of events that may contribute to adverse operating conditions. The specified events include resource shortages, demand increases, and equipment unavailability. Screening probabilities depend on the tree structure, event definitions, and assumed input probabilities. Service shortfalls are evaluated separately using the simulated service trajectories.

An AND-gate output occurs when all its input events occur. Equation (10) gives the output probability when the basic events entering the gate are mutually independent.

$$P(A) = \prod_{j=1}^{n} P\left(E_j\right) \tag{10}$$

where

- $P(A)$ = probability of the AND-gate output event A;
- $P(E_j)$ = probability of basic event Ej;
- $j$ = basic-event index and;
- $n$ = number of basic events entering the AND gate.

An AND gate can represent the simultaneous unavailability of battery and fuel-cell support. Whether this combination produces a service shortfall also depends on the remaining generation and service demand. Deterministic disturbance simulations assess service consequences under the prescribed operating conditions.

2.3.10. Fault OR-Gate Probability

An OR-gate output occurs when at least one of its input events occurs. In this study, OR gates represent alternative adverse conditions, including equipment unavailability, resource shortages, and storage-related events. Equation (11) gives the output probability for mutually independent basic events.

$$P(A) = 1 - \prod_{j=1}^{n}\left[1 - P\left(E_j\right)\right] \tag{11}$$

where

- $P(A)$ = probability of the OR-gate output event $A$;
- $P(E_j)$ = probability of basic event $E_j$;
- $j$ = basic-event index; and
- $n$ = number of basic events entering the OR gate.

The product expressions in Equations (10) and (11) require mutual independence among the gate inputs. Even when distinct basic events are independent, intermediate branches may be dependent if they share a basic event. The complete Boolean expression is therefore evaluated by state enumeration. Each basic event is assigned a single state within each enumerated combination, preserving consistency across branches in which it appears.

Modelling assumptions: Independence among distinct basic events defines the reference case. Event probabilities are assumed screening inputs. Adjustments based on service coverage or storage conditions provide scenario conditioning rather than empirical calibration. The inputs have not been calibrated against operating records or defined over a common observation period. The resulting probabilities therefore have no established interpretation as daily failure probabilities. Selected departures from independence are examined through dependence sensitivity tests.

Fault-tree implementation and structural review: The original fault tree contains 14 inputs covering resource shortages, demand increases, equipment unavailability, storage depletion, cascading effects, environmental stress, control failure, maintenance unavailability, external supply disruption, forecast deviation, and multi-service stress. These inputs include operating conditions and demand changes, as well as equipment events. Component mean time between failures alone cannot therefore determine all input probabilities. Separate failure events for the PEM electrolyzer, WTE subsystem, MED subsystem, and absorption chiller are not explicitly represented.

The structural review evaluates a second tree containing 11 inputs. Storage depletion, cascading failure, and multi-service stress are excluded as independent basic-event inputs because they can arise from interacting system conditions. Their service consequences are examined through the simulated trajectories. Results for the 11-input structure are reported separately from the original 14-input baseline. Both calculations remain conditional on their respective tree structures and probability assumptions. Possible overlap among the retained events and their relationship to actual service failure require supporting evidence.

Dependence Sensitivity: The tests examine two event pairs: low photovoltaic output with low wind output, and battery unavailability with fuel-cell unavailability. For each pair, the joint distribution combines an independent construction with a shared-uniform construction while preserving the specified marginal probabilities. Mixture weights of 0.25, 0.50, and 1.00 are evaluated for each pair separately and for both pairs together. A weight of zero reproduces independence. A weight of one gives the maximum positive dependence permitted by the specified pair marginals.

The screening probability is recalculated by Boolean-state enumeration for each setting. The mixture weights are prescribed sensitivity parameters rather than measured correlation coefficients. The results describe sensitivity to the tested dependencies between these two pairs. Dependencies involving other event combinations are outside these tests, so the analysis does not constitute a comprehensive common-cause failure assessment.

#### 2.3.11. Event Tree Analysis (ETA)

Event tree analysis (ETA) provides a conceptual framework for organizing possible responses to an initiating disturbance. It distinguishes the initiating event from subsequent detection, control, protection, and restoration actions. Equation (12) expresses pathway probability as the initiating-event probability multiplied by the conditional probabilities of

successive barrier outcomes. It is retained as a reference formulation and is not numerically evaluated in this study. ETA identifies possible response pathways and the evidence needed to assess their probabilities and barrier effectiveness.

$$P(\text{path}_k) = P(I)\prod_{j=1}^{m} P\left(B_j^{(k)} \middle| I, B_1^{(k)}, \ldots, B_{j-1}^{(k)}\right) \quad (12)$$

where

- $P(path_k)$ = probability of event-tree outcome pathway k;
- $P(I)$ = probability of the initiating disturbance;
- $B_j^{(k)}$ = success or failure outcome of barrier j along pathway k;
- $P\left(B_j^{(k)} \mid I, B_1^{(k)}, \ldots, B_{j-1}^{(k)}\right)$ = conditional probability of the barrier outcome given the initiating event and preceding outcomes;
- $m$ = total number of barriers considered; and
- $k$ = event-tree pathway index.

Implementation and modelling assumptions: The deterministic simulations examine the consequences of prescribed conditions, including battery failure, fuel-cell availability constraints, and alternative dispatch limits. They evaluate dispatch behaviour, storage utilization, service shortfalls, and consistency between storage inventories and flows. These simulations do not estimate barrier-success or event-tree pathway probabilities. Restoration of subsystem availability follows a prescribed schedule. Equipment repair times and the effectiveness of detection, protection, and repair actions are not inferred from the dispatch results.

#### 2.3.12. Maximum Performance Loss

Maximum performance loss measures the greatest relative reduction in multi-service performance over the specified assessment interval. Equation (13) uses ISPS as the time-dependent performance measure and compares its minimum value with the pre-disturbance reference. Multiplying the result by 100 gives the percentage reduction. The numerator gives the absolute ISPS reduction, which is reported separately.

$$\Delta P_{\max} = \frac{P_0 - \min\limits_{t_d \le t \le t_b} P(t)}{P_0} \quad (13)$$

where

- $\Delta P_{\max}$ = maximum performance loss (dimensionless);
- $P_0$ = pre-disturbance system performance (dimensionless);
- $P(t)$ = system performance at time t, represented by the ISPS (dimensionless);
- $t_d$ = disturbance initiation time (h);
- $t_b$ = end of the specified assessment interval (h); and
- $t$ = simulation time within the specified assessment interval (h).

Modelling assumptions: The pre-disturbance reference performance must be positive ($P_0 > 0$). Comparisons across cases use the same reference-selection procedure and assessment interval. The endpoint is specified independently of whether service coverage returns to baseline. A minimum ISPS below the reference produces a positive loss, while equality gives zero. If the minimum exceeds the reference, the expression is negative and indicates a performance gain.

#### 2.3.13. Service Restoration Time

Service restoration time measures the elapsed time from disturbance onset to the start of an interval in which all four service-coverage indicators satisfy the specified baseline crite-

rion. The required persistence duration must be completed before restoration is confirmed. Full planned-service satisfaction and reserve replenishment are assessed separately.

$$T_R = t_r - t_d \tag{14}$$

where

- $T_R$ = elapsed time from disturbance onset to the start of the qualifying interval (h);
- $t_r$ = start time of the interval during which all four service-coverage indicators satisfy the baseline criterion for the required duration (h); and
- $t_d$ = time at which the prescribed disturbance begins (h).

Modelling assumptions: The baseline threshold, numerical tolerance, and persistence duration are specified for each assessment. Service restoration is confirmed only when every service-coverage indicator satisfies the threshold continuously for the required duration. The reported time refers to the start of that qualifying interval. If no qualifying interval is completed within the simulation, return to baseline coverage is reported as not demonstrated. The prescribed disturbance duration follows the availability schedule and is reported separately. Scheduled input restoration does not establish physical equipment repair, restart, or replenishment of stored reserves.

#### 2.3.14. Cumulative Performance Loss

Cumulative performance loss accounts for both the magnitude and duration of changes in multi-service performance. Equation (15) integrates the difference between the pre-disturbance reference and the simulated ISPS over the specified assessment interval. When ISPS remains at or below the reference, a larger value indicates a deeper or more prolonged shortfall. The integral is signed, so performance above the reference offsets deficits below it.

$$L_R = \int_{t_d}^{t_b} [P_0 - P(t)]dt \tag{15}$$

where

- $L_R$ = cumulative signed performance loss over the specified assessment interval (ISPS·h);
- $P_0$ = system performance immediately before the disturbance;
- $P(t)$ = system performance at time t, represented by the ISPS;
- $t_d$ = time at which the disturbance begins (h);
- $t_b$ = end of the specified assessment interval (h); and
- $t$ = time within the specified assessment interval (h).

Modelling assumptions: The pre-disturbance reference and assessment interval are specified for each calculation. Comparisons across cases use the same reference-selection procedure, assessment duration, and integration convention. The result describes performance over the specified observation window, regardless of whether return to baseline service coverage is demonstrated.

#### 2.3.15. Disturbance-Period Performance Preservation Index (DPPI)

The Disturbance-Period Performance Preservation Index (DPPI) compares average ISPS during the prescribed disturbance window with the pre-disturbance reference. Equation (16) calculates this ratio from disturbance onset to the scheduled end of the disturbance. A value of one indicates that average performance equals the reference. A value below one indicates a net performance deficit, while a value above one indicates average performance above the reference. DPPI is interpreted alongside individual service coverage, critical-service shortfalls, and storage trajectories.

$$\mathrm{DPPI} = \frac{1}{P_0(t_b - t_d)} \int_{t_d}^{t_b} P(t)\,\mathrm{d}t \tag{16}$$

where

- DPPI = Disturbance-Period Performance Preservation Index (dimensionless);
- $P_0$ = system performance immediately before the disturbance;
- $P(t)$ = system performance at time t, represented by the ISPS;
- $t_d$ = time at which the disturbance begins;
- $t_b$ = end of the specified assessment interval (h); and
- $t$ = time within the specified assessment interval (h).

Modelling assumptions: The calculation requires $P_0 > 0$ and $t_b > t_d$. Comparisons use consistently defined disturbance windows and the same reference-selection procedure. DPPI measures performance preservation under prescribed availability signals. It does not quantify an independently modelled physical restoration process or represent a probability of successful recovery. Return to baseline service coverage and replenishment of stored reserves are assessed separately.

#### 2.3.16. Eight-State Descriptive Framework

The eight-state descriptive framework classifies operating conditions and response phases using service adequacy, critical-service requirements, reserve conditions, and recorded operational actions. The states are Normal, Stressed, Adapted, Degraded, Severe, Emergency Recovery, Repair Restoration, and Recovered. A classification is assigned only when the required information is available at the evaluated time. The framework does not use a transition-rate matrix or predict future state-occupancy probabilities.

#### 2.3.17. Service-Adequacy Indicators

Planned-service adequacy is evaluated using the individual coverage indicators defined in Equation (6). All planned requirements are satisfied when every coverage indicator reaches one within the specified numerical tolerance. Otherwise, at least one planned-service shortfall is recorded. Classification uses individual indicators so that stronger performance in one service cannot conceal a shortfall in another.

Critical-service adequacy is evaluated using Equation (9). Equation (17) identifies the minimum coverage across services with specified critical requirements.

$$C_{\text{crit,min}}(t) = \min_{i \in \mathcal{K}} C_{i,\text{crit}}(t) \tag{17}$$

where

- $C_{\text{crit,min}}(t)$ = minimum critical-service coverage at time t (dimensionless);
- $C_{i,\text{crit}}(t)$ = critical-service coverage for service i, as defined in Equation (9);
- $\mathcal{K}$ = set of services with specified critical requirements;
- $i$ = service index; and
- t = simulation time (h).

Critical requirements are satisfied when the minimum coverage reaches one within the specified numerical tolerance. A value below this tolerance-adjusted threshold identifies at least one critical-service shortfall. Missing required indicators prevent confirmation that all critical requirements are satisfied.

Inventory requirements are assessed separately using quantities expressed in consistent units. Hydrogen-reserve adequacy compares actual stored hydrogen mass with the specified reserve requirement. Hydrogen-production coverage is not substituted for stored inventory. Where total village electricity served is compared with a critical-load threshold, the result remains an aggregate adequacy proxy. Confirmation of delivery to individual critical facilities requires explicit allocation information.

#### 2.3.18. Reserve Conditions and Response Flags

Reserve adequacy distinguishes Normal from Stressed operation when planned and critical-service requirements are satisfied and no response phase takes precedence. The reserve indicator, calculation basis, and target are specified for each evaluated configuration. Electrical supply headroom, battery state of charge, and hydrogen inventory are assessed separately because they describe different aspects of backup capability.

Operational actions and confirmation of the post-disturbance criterion are represented by the following binary flags:

- $a(t)$ = adaptation action active at time $t$;
- $e(t)$ = emergency response active at time $t$;
- $r(t)$ = repair or restoration action active at time $t$; and
- $g(t)$ = specified post-disturbance recovery condition explicitly confirmed at time $t$;

Here, $t$ denotes simulation time in hours. For the action flags, a value of 1 indicates that the corresponding action is explicitly recorded as active, while 0 indicates that it is explicitly inactive. For $g(t)$, a value of 1 indicates that the specified criterion has been confirmed, while 0 indicates that it has been evaluated but not met. Missing information remains unspecified and is not assigned a value of zero. An increase in ISPS alone does not establish an operational action or justify assignment of the Recovered state.

#### 2.3.19. State-Classification Criteria

Table 1 defines the classification criteria and provides examples of actions associated with the response states. In the simulations, the energy management system (EMS) dispatches the battery and fuel cell within their operating limits. Battery dispatch depends on the power request and state of charge, while fuel-cell output depends on the power request, rated capacity, and accessible hydrogen inventory. The EMS allocates power first to village electricity, followed by freshwater production, cooling, and hydrogen production. State assignment requires evidence from the simulation or operational records that the relevant conditions and actions are present. The availability schedule specifies when subsystem availability is restored. Classification of protective isolation or component repair requires explicit evidence of the corresponding action.

**Table 1.** State classification criteria for the eight-state descriptive framework.

| State | Service and Reserve Criteria | Response Condition |
|---|---|---|
| Normal | All planned and critical-service requirements are met, and the specified reserve target is met. | The EMS maintains routine service allocation. Disturbance-related adaptation, emergency response, repair, and the confirmed post-disturbance phase are inactive. |
| Stressed | All planned and critical-service requirements are met, but the reserve level is below the specified target. | Routine operation continues. Disturbance-related adaptation, emergency response, repair, and the confirmed post-disturbance phase are inactive. |
| Adapted | At least one planned-service requirement is unmet, and all critical-service requirements are met. | The EMS applies a documented adjustment, such as load prioritization, modified battery dispatch, or fuel-cell support. Emergency and repair actions are inactive. |
| Degraded | At least one planned-service requirement is unmet, and all critical-service requirements are met. | Planned-service shortfalls persist under routine dispatch and service allocation. Adaptive, emergency, and repair actions are inactive. |

**Table 1.** *Cont.*

| State | Service and Reserve Criteria | Response Condition |
| --- | --- | --- |
| Severe | At least one critical-service requirement is unmet, or a required inventory threshold is breached. | Emergency and repair phases take precedence when active. Any ongoing adaptation is reported separately. |
| Emergency Recovery | Planned or critical-service requirements may remain unmet. Service coverage and reserves are assessed separately. | A designated emergency action is active, such as emergency load shedding, protective isolation, or prioritization of essential loads. Repair is inactive. |
| Repair Restoration | Service provision may remain partial. Planned-service coverage, critical-service adequacy, and reserves are assessed separately. | A designated repair or restoration action is active, such as component repair, reconnection, or staged return to service. Emergency response is inactive |
| Recovered | All planned and critical-service requirements are met, required inventory thresholds are satisfied, and the specified post-disturbance service criterion is confirmed. Battery and hydrogen reserve replenishment is assessed separately. | Emergency and repair actions have ended. Reserve replenishment is reported separately. |

#### 2.3.20. Classification Procedure

The assessment first checks whether the required service, inventory, reserve, and response information is available and consistent. An active emergency or repair phase takes precedence over the service-based operating states. Critical-service status is reported separately. If both phases are active, the assessment applies the specified precedence rule. If no precedence rule is specified, the classification is recorded as Unresolved.

With emergency and repair actions inactive, the system is classified as Recovered when all planned and critical-service requirements are met, required inventory thresholds are satisfied, and the specified post-disturbance criterion is confirmed. For other operating conditions, a critical-service shortfall or a breach of a required inventory threshold leads to a Severe classification. If critical-service and inventory requirements are met but a planned-service shortfall remains, the adaptation flag distinguishes Adapted from Degraded.

When all planned and critical-service requirements are met, required inventory thresholds are satisfied, and disturbance-related adaptation is inactive, the specified reserve target distinguishes Normal from Stressed. Conditions that do not satisfy any defined state criterion are recorded as Unresolved. Missing or inconsistent information needed for classification also results in an Unresolved assessment. Unresolved is an assessment status separate from the eight operating states.

#### 2.3.21. Modelling Assumptions and Interpretation

The assessment specifies the service thresholds, numerical tolerances, reserve definition and target, and post-disturbance service criterion for each configuration. The state labels describe modelled operating conditions and recorded response actions. Emergency Recovery and Repair Restoration identify active response phases.

Predefined software tests use constructed inputs to check whether the classification rules assign the expected label for all eight states. These tests verify the classification logic; they do not demonstrate that every state occurred in the disturbance simulations. A complete state trajectory is reported only when the required indicators and response flags are available at every evaluated time.

### 2.4. Integrated Disturbance-Response Assessment

The assessment combines operating cases from MG-OPT with time-dependent simulations in MATLAB/Simulink. At each simulation step, the model uses supply and demand for electricity, freshwater, hydrogen production, and cooling to calculate individual service coverage and the Integrated Service Performance Score (ISPS). Critical-service requirements are evaluated separately. The model also records battery state of charge, hydrogen inventory, and fuel-cell output. Electrical power-balance and storage stock–flow checks assess the numerical consistency of the four simulated operating cases. The implementation uses simulated trajectories for offline assessment. Continuous measurements from an operating physical system, real-time synchronization, and online calibration are outside the study's scope.

During a disturbance, the ISPS provides the performance trajectory, $P(t)$. Equations (13), (15), and (16) give the maximum relative performance loss, cumulative signed performance loss, and Disturbance-Period Performance Preservation Index (DPPI), respectively. Maximum and cumulative performance loss are evaluated over their specified assessment intervals. The DPPI uses the prescribed disturbance window. Equation (14) gives the elapsed time from disturbance onset to the start of an interval in which every service meets the specified baseline coverage criterion. Restoration is confirmed after this condition persists for the required duration, subject to the specified numerical tolerance. Individual coverage indicators are reported alongside the ISPS to identify service-specific shortfalls.

Fault Tree Analysis (FTA) screens specified event combinations involving resource shortages, equipment unavailability, storage limitations, and service disruptions. Event probabilities without empirical support are treated as assumed screening inputs. Dependence sensitivity tests examine selected departures from independence, while Monte Carlo parameter propagation evaluates variation arising from the prescribed input-probability distributions. The 19 additional disturbance scenarios are assessed through these screening calculations and are not additional time-dependent simulations. Event Tree Analysis (ETA) organizes possible response pathways conceptually. The eight-state descriptive framework assigns states where the required service, inventory, reserve, and response information is available.

### 2.5. Disturbance-Response and Backup Dispatch Strategy

The disturbance-response strategy coordinates available generation, battery storage, hydrogen storage, and fuel-cell support. During an electrical deficit, the energy management system (EMS) dispatches the battery first, subject to its power and state-of-charge limits. The fuel cell can supply part or all of the remaining power request, subject to its rated capacity and accessible hydrogen inventory. Because the four services share resources, an electrical deficit can affect freshwater production, cooling, and hydrogen production alongside village electricity supply.

The assessment tracks battery state of charge, hydrogen inventory, fuel-cell output, individual service coverage, and the Integrated Service Performance Score (ISPS). These trajectories cover the prescribed disturbance and the subsequent observation period. Performance is compared with the pre-disturbance reference to quantify the magnitude and duration of degradation. The availability schedule determines when the imposed constraints are removed. The assessment then checks whether individual service coverage meets the baseline criterion defined for Equation (14). Table 2 summarizes the disturbance conditions, modelled responses, monitored variables, and assessment measures.

**Table 2.** Disturbance-response and service-performance assessment strategy.

| Disturbance or Operating Conditions | Model Response | Monitored Variables | Assessment Measures |
| --- | --- | --- | --- |
| Reduced renewable generation | Lower available PV and wind generation can create an electrical deficit. The EMS dispatches the battery within its power and state-of-charge (SOC) limits, followed by fuel-cell support where available. | Available PV and wind power, electrical demand, battery power and SOC, fuel-cell output, and hydrogen inventory. | Changes in electricity-service coverage and ISPS, including the magnitude and duration of degradation. |
| WTE/biogas unavailability | The EMS dispatches the battery within its power and SOC limits. The fuel cell can supply the remaining power request within its rated capacity and accessible hydrogen inventory. | WTE/biogas power, total electrical generation, battery power and SOC, fuel-cell output, hydrogen inventory, and electricity-service coverage. | Changes in service coverage during the compound disturbance. The individual contribution of WTE/biogas unavailability is evaluated only where a separate comparison case is available. |
| PEM electrolyzer derating | Reduced electrolyzer availability limits hydrogen production. Stored hydrogen is tracked separately because the fuel cell can draw on the remaining inventory. | Electrolyzer availability, hydrogen production rate, hydrogen demand, and stored hydrogen inventory. | Reduction in hydrogen-production coverage and the remaining hydrogen inventory available for backup electricity generation. |
| Electrical supply deficit | The EMS dispatches the battery first, followed by fuel-cell support. Dispatch remains subject to battery power and SOC limits, fuel-cell rated capacity, and accessible hydrogen inventory. | Electrical deficit, battery power and SOC, fuel-cell power request and output, and stored hydrogen inventory. | Electricity-service continuity, storage utilization, and changes in freshwater, cooling, and hydrogen-production coverage. |
| Compound disturbance | The simulation simultaneously reduces renewable generation and WTE/biogas availability and derates the PEM electrolyzer. These constraints affect several generation and conversion pathways. | Individual service-coverage indicators, battery SOC, stored hydrogen inventory, fuel-cell output, and ISPS. | Service shortfalls, shortfalls relative to the critical electrical-load proxy, maximum and cumulative performance loss, and the Disturbance-Period Performance Preservation Index (DPPI). |
| Post-disturbance restoration | The imposed availability constraints are removed at the scheduled endpoint. Subsequent trajectories show the simulated response to restored inputs. | Individual service coverage, ISPS, generation outputs, battery SOC, and hydrogen inventory | Return to baseline service coverage, confirmed when every service meets the specified criterion for the required duration. Service restoration time is measured to the start of the qualifying interval. Reserve replenishment is assessed separately. |

The simulated response depends on available generation, stored energy, conversion capacity, and operating limits. Return to baseline service coverage following scheduled input restoration does not establish full planned-service satisfaction, reserve replenishment, or physical equipment recovery.

## 3. Integrated Simulation for HES Performance Assessment

### *3.1. Integrated Simulation Workflow*

The proposed hybrid energy system is analysed using an integrated modelling and simulation workflow comprising MG-OPT, HOMER, and MATLAB/Simulink as shown in Figure 3. The workflow combines multigeneration system analysis, cross-platform comparison, time-dependent simulation, and conditional probabilistic screening. MG-OPT evaluates candidate configurations, component capacities, resource pathways, and interactions among electricity, freshwater, hydrogen production, and cooling. HOMER supports comparison of component configurations and performance quantities represented in both platforms. MATLAB/Simulink examines service delivery, storage behaviour, dispatch, and disturbance response using the implemented conversion relationships and operating constraints.

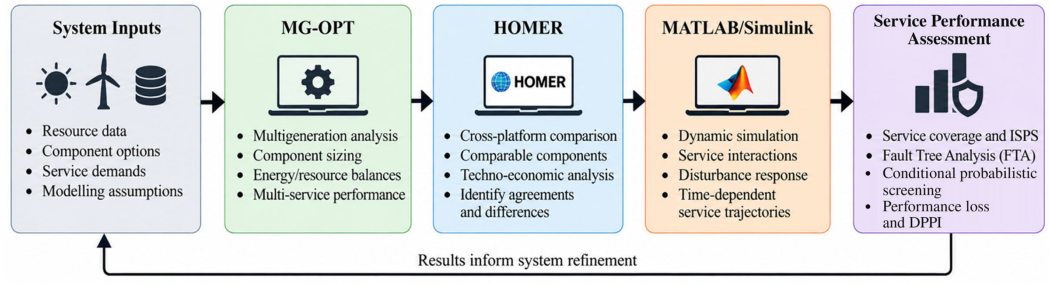


**Figure 3.** Integrated modelling and simulation workflow for the proposed Hybrid energy system.

MATLAB/Simulink provides the service and storage trajectories used in the assessment framework described in Section 2. Individual service coverage and the Integrated Service Performance Score (ISPS) characterize service adequacy. Maximum performance loss, cumulative performance loss, and the Disturbance-Period Performance Preservation Index (DPPI) quantify disturbance consequences over specified assessment intervals. Service restoration time is reported when individual service coverage satisfies the defined baseline criterion for the required duration.

Fault Tree Analysis (FTA), dependence sensitivity tests, and Monte Carlo parameter propagation provide complementary screening under stated probability assumptions. The eight-state descriptive framework supports classification where the required service, inventory, reserve, and response information is available. Sections 3.2–3.4 describe the modelling stages. Section 4 presents the case-specific parameters and implementation, and Section 5 reports the quantitative results.

### *3.2. MG-OPT Multigeneration System Analysis*

This study builds on the Microgrid Optimization framework developed by Gabbar and Hemied [25]. Its renewable-energy and hydrogen optimization approach is adapted to the Gbamu-Gbamu case study, with the assessment extended to electricity, freshwater, hydrogen production, and cooling. In this study, MG-OPT denotes the Multi-Generation Optimization Framework used for this extended assessment. The framework represents renewable and dispatchable generation, battery and hydrogen storage, and energy-conversion technologies. Resource availability, service requirements, candidate component capaci-

ties, conversion efficiencies, storage characteristics, and operating constraints define the evaluated configurations.

Candidate configurations and technology parameters are varied to examine their effects on resource utilization, conversion performance, and individual service outputs. Because the four services share electrical, thermal, and storage resources, a change that benefits one service may affect another. Electricity, freshwater, hydrogen, and cooling outputs are therefore reported individually to identify cross-service trade-offs.

The resulting component capacities, energy and resource balances, storage requirements, and service outputs inform the subsequent modelling stages. Supported configurations and performance quantities are compared independently in HOMER. MATLAB/Simulink evaluates the selected architecture through time-dependent storage balances, dispatch, and service delivery under prescribed disturbances. Return to baseline service coverage is assessed using the specified restoration criterion. HOMER provides a cross-platform comparison rather than experimental validation. Case-specific inputs, technology sensitivities, and quantitative results are presented in Sections 4 and 5.

#### 3.2.1. MG-OPT Computational Procedure and Reproducibility

In this study, MG-OPT denotes the modelling workflow implemented in MATLAB R2026a Update 5 and Python 3.13.18, with the Python code executed in Google Colab. The Python-based electricity–hydrogen component uses mixed-integer linear programming (MILP), implemented through PuLP (https://www.coin-or.org/pulp/) and the CBC solver (https://github.com/coin-or/Cbc) over a 24 h operating horizon. It considers operating costs, emissions, energy utilization, and surplus-energy value, subject to power-balance, component-capacity, and storage constraints.

The MATLAB component evaluates electricity, freshwater, hydrogen, and cooling outputs using component-performance equations and predefined operating cases. These comparisons characterize the evaluated configurations and their service trade-offs without establishing global optimality across all possible configurations. The mathematical relationships are presented below, while the model inputs and results are reported in Sections 4 and 5.

#### 3.2.2. Optimization Objective Function

The Python-based electricity–hydrogen optimization minimizes a weighted objective combining operating costs, emissions, energy utilization, and surplus electricity and hydrogen value. The negative signs reward higher energy utilization and surplus value within the minimization objective.

$$\min Z = w_c C + w_e E - w_u U - w_p \Pi \tag{18}$$

where

- $Z$ = weighted objective value;
- $C$ = net system cost over the optimization horizon, after deducting surplus revenue;
- $E$ = total emissions over the optimization horizon;
- $U$ = modelled energy-utilization term;
- $\Pi$ = value assigned to surplus electricity and hydrogen; and
- $w_c$, $w_e$, $w_u$, and $w_p$ = corresponding objective weights.

The model calculates $U$ by summing photovoltaic, wind, and fuel-cell electrical output over the 24 1-h intervals. This quantity represents combined electrical energy output rather than an energy-efficiency ratio. Surplus revenue, $\Pi$, is calculated from surplus electricity and hydrogen sales using the valuation parameters specified in the model. The function defines default objective weights of 0.25 for all four terms. No normalization is applied, so

equal numerical weights do not imply equal contributions to the objective. Because $C$ already deducts surplus revenue, its effective reward in Equation (18) is $w_c + w_p$. Grid-related emissions are zero under the imposed islanded-operation constraint.

#### 3.2.3. Electrical Power Balance

Equation (19) balances electrical supply and allocation at each hourly optimization step. Supply includes photovoltaic generation, wind generation, fuel-cell output, battery discharge, and grid imports where available. Electricity is allocated to community demand, electrolysis, electric-vehicle charging, battery charging, and surplus output. Grid imports are fixed at zero for the islanded configuration.

$$P_{\mathrm{PV},t} + P_{\mathrm{WT},t} + P_{\mathrm{FC},t} + P_{\mathrm{bat,dis},t} + P_{\mathrm{grid},t} = P_{\mathrm{load},t} + P_{\mathrm{EL},t} + P_{\mathrm{EV},t} + P_{\mathrm{bat,ch},t} + P_{\mathrm{sur},t} \quad (19)$$

where:

- $P_{\mathrm{PV},t}$ = photovoltaic power generation at time step $t$ (kW);
- $P_{\mathrm{WT},t}$ = wind power generation at time step $t$ (kW);
- $P_{\mathrm{FC},t}$ = fuel-cell electrical output at time step $t$ (kW);
- $P_{\mathrm{bat,dis},t}$ = battery discharge power at time step $t$ (kW);
- $P_{\mathrm{grid},t}$ = grid import power at time step $t$, fixed at zero for islanded operation (kW);
- $P_{\mathrm{load},t}$ = community electricity demand at time step $t$ (kW);
- $P_{\mathrm{EL},t}$ = electrolyzer electricity consumption at time step t (kW);
- $P_{\mathrm{EV},t}$ = electric-vehicle charging power at time step $t$ (kW);
- $P_{\mathrm{bat,ch},t}$ = battery charging power at time step $t$ (kW);
- $P_{\mathrm{sur},t}$ = surplus electrical power at time step $t$ (kW); and
- $t$ = hourly optimization time index.

#### 3.2.4. Battery Storage Dynamics

Equation (20) updates battery stored energy between consecutive hourly time steps. It accounts for charging and discharging power and their respective conversion efficiencies.

$$B_{t+1} = B_t + \eta_{\mathrm{ch}} P_{\mathrm{ch},t} \Delta t - \frac{P_{\mathrm{dis},t} \Delta t}{\eta_{\mathrm{dis}}} \quad (20)$$

where:

- $B_{t+1}$ = battery stored energy at the next time step (kWh);
- $B_t$ = battery stored energy at the current time step (kWh);
- $\eta_{\mathrm{ch}}$ = battery charging efficiency (dimensionless);
- $\eta_{\mathrm{dis}}$ = battery discharging efficiency (dimensionless);
- $P_{\mathrm{ch},t}$ = battery charging power at time step $t$ (kW);
- $P_{\mathrm{dis},t}$ = battery discharging power at time step $t$ (kW); and
- $\Delta t$ = optimization time-step duration, equal to 1 h.

The charging and discharging powers correspond to $P_{\mathrm{bat,ch},t}$ and $P_{\mathrm{bat,dis},t}$ in Equation (19). The model applies bounds on stored energy and charging and discharging power. A cyclic constraint requires the final stored energy to equal its initial value, preventing net depletion of the battery over the 24 h optimization horizon.

#### 3.2.5. Hydrogen Storage Dynamics

Equation (21) updates the stored hydrogen inventory between consecutive hourly time steps. It adds the hydrogen entering the tank and subtracts the hydrogen withdrawn during each interval.

$$H_{t+1} = H_t + H_{\mathrm{ch},t} - H_{\mathrm{dis},t} \quad (21)$$

where:

- $H_{t+1}$ = hydrogen inventory at the next time step (kg);
- $H_t$ = hydrogen inventory at the current time step (kg);
- $H_{\mathrm{ch},t}$ = hydrogen mass added to storage during time step $t$ (kg);
- $H_{\mathrm{dis},t}$ = hydrogen mass withdrawn from storage during time step $t$ (kg); and
- $t$ = hourly optimization time index.

The charging and withdrawal terms represent masses transferred during each one-hour interval, so no additional time-step multiplier is required in Equation (21). The model constrains inventory to remain between zero and the tank capacity and limits hydrogen charging and withdrawal. Binary variables prevent simultaneous charging and withdrawal. A cyclic constraint requires the final hydrogen inventory to equal its initial value, preventing net depletion of stored hydrogen over the 24 h optimization horizon.

#### 3.2.6. Cyclic Storage Constraints

Equation (22) requires battery stored energy and hydrogen inventory to equal their initial values at the end of the 24 h optimization horizon. These constraints prevent the optimized daily schedule from relying on net depletion of either storage resources.

$$B_{24} = B_0, \;\; H_{24} = H_0 \tag{22}$$

where:

- $B_{24}$ = battery-stored energy at the end of the 24 h optimization horizon (kWh);
- $B_0$ = initial battery-stored energy (kWh);
- $H_{24}$ = hydrogen inventory at the end of the 24 h optimization horizon (kg); and
- $H_0$ = initial hydrogen inventory (kg).

These constraints require battery stored energy and hydrogen inventory to return to their initial levels at the end of the Python optimization period. In the separate MATLAB/Simulink disturbance simulations, storage replenishment is assessed by tracking battery energy and hydrogen inventory.

#### 3.2.7. Four Service Multigeneration Assessment

The MATLAB-based MG-OPT framework evaluates electricity, freshwater, hydrogen production, and cooling under different operating conditions. It uses component–performance relationships, energy and material balances, and predefined configurations to calculate service outputs.

For each configuration, service outputs are compared with the corresponding community requirements. Equation (6) calculates individual service coverage as the ratio of supply to demand, capped at one. A value of one indicates that the requirement is met, while a lower value indicates a shortfall. Equation (7) combines these indicators into the Integrated Service Performance Score (ISPS), assigning each service a weight of 0.25. Individual coverage values are reported alongside the ISPS to identify service-specific shortfalls. These assessment weights are separate from the service priorities used by the energy management system.

The MATLAB assessment examines predefined operating modes, technology variations, community applications, and performance objectives. Configurations are compared using individual service outputs, integrated efficiency, resource utilization, and other specified performance indicators. These comparisons identify technical differences and cross-service trade-offs without establishing global optimality across all possible configurations.

The Python-based MILP determines electricity–hydrogen operating schedules under its objective function and constraints. The MATLAB assessment evaluates specified four-service configurations using component-performance relationships and operating-case

comparisons. These are complementary modelling stages with distinct formulations and assumptions. Their outputs inform the subsequent HOMER cross-platform comparisons and MATLAB/Simulink disturbance-response assessments.

### *3.3. HOMER Cross-Platform Comparison Method*

HOMER provides a separate modelling environment for comparing components and performance quantities represented in the MG-OPT analysis. This stage examines system feasibility under HOMER's component representations, sizing procedures, dispatch assumptions, and operating constraints. It provides a cross-platform comparison rather than experimental validation of MG-OPT or MATLAB/Simulink.

The HOMER configuration in Figure 4 includes the GeoORC_Kalina generator as an equivalent representation of the geothermal Organic Rankine Cycle (ORC) and Kalina cycle pathway. The MATLAB reference geothermal electrical output of 1263 kW informs this representation. This value is a modelling input and does not establish geothermal resource availability at the case-study location.

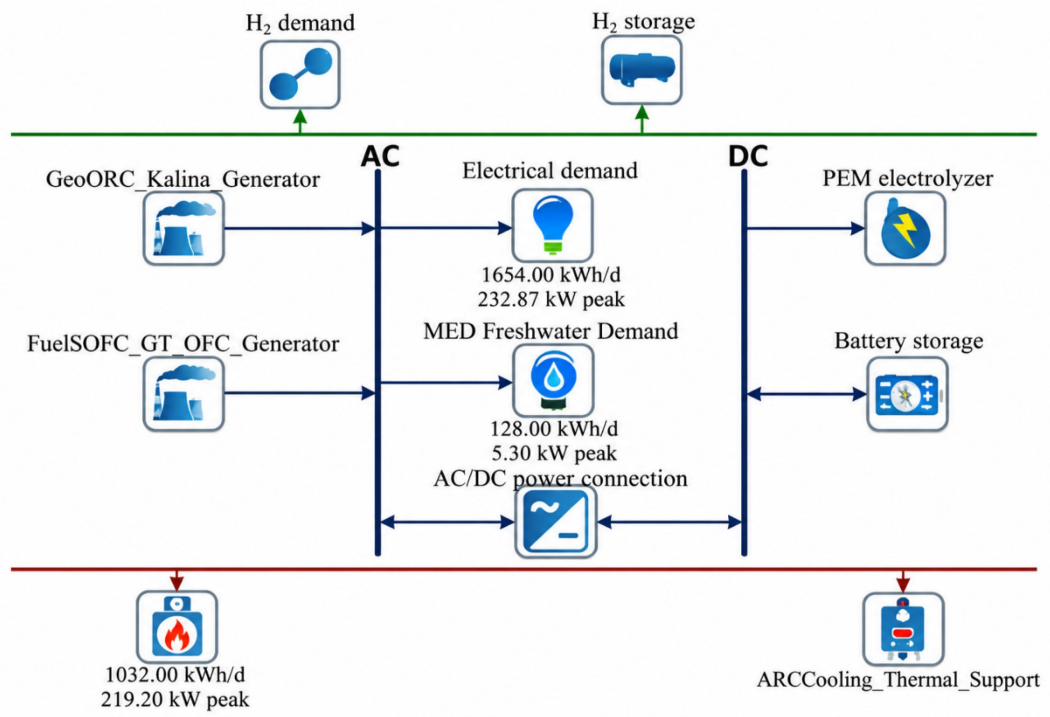


**Figure 4.** HOMER system configuration used for cross-platform assessment.

The generator connects to the AC bus and can support community electrical loads, electrolyzer operation, and battery charging through the relevant conversion equipment. HOMER represents this pathway as an equivalent electrical generator. The comparison therefore examines electrical capacity and energy contribution without reproducing the detailed ORC and Kalina thermodynamics.

The comparison uses sequential and independent workflows. In the MATLAB/MG-OPT-to-HOMER workflow, selected capacities, operating requirements, and demand profiles define corresponding HOMER cases. These cases assess feasibility and economic performance within the specified component search ranges. In the HOMER-to-MATLAB workflow, selected configurations and operating assumptions inform the evaluation of technology performance and interactions among the four services. The independent workflow evaluates comparable conditions in both environments without requiring identical internal formulations.

Where equivalent representations are available, the comparison considers resource conditions, electrical demand, generation capacity, storage capacity, conversion equipment, and economic assumptions. The assessed quantities include energy balances, generation and storage requirements, system feasibility, and techno-economic performance. Differences in dispatch, component representations, search limits, and model boundaries are considered when interpreting the results.

Hydrogen production and storage are compared where equivalent components and consistent assumptions are available. Freshwater production, cooling, detailed thermodynamics, and disturbance-response indicators outside the shared modelling scope are assessed separately. HOMER identifies feasibility and capacity constraints under its configured assumptions, while MATLAB/Simulink evaluates time-dependent service delivery and storage behaviour during prescribed disturbances. Section 4 presents the case-specific settings and component limits, and Section 5 reports the cross-platform results.

#### 3.3.1. HOMER Simulation Formulation

HOMER Pro evaluates the technical feasibility and lifecycle economic performance of candidate hybrid energy systems using its built-in component models, simulation procedures, and optimization algorithms. Configurations are assessed under specified resource profiles, demand requirements, component capacities, dispatch settings, and operating constraints. This formulation is separate from the Python-based electricity–hydrogen MILP described in Section 3.2. Among configurations that satisfy the specified constraints, HOMER identifies the option with the lowest total net present cost (NPC) within the investigated search space [26]. This objective is expressed in Equation (23).

$$\min_{\mathbf{x}\in\mathcal{F}} C_{\mathrm{NPC}}(\mathbf{x}) \tag{23}$$

where:

- x = vector defining a candidate system configuration and its component sizes;
- $\mathcal{F}$ = set of feasible configurations within the specified search space and operating constraints; and
- $C_{\mathrm{NPC}}(\mathrm{x})$ = total net present cost of configuration $\mathbf{x}(\$)$.

NPC accounts for applicable lifecycle costs, including capital, replacement, operation and maintenance, and fuel costs. Salvage value and applicable revenues are deducted. Equation (24) relates NPC to the total annualized system cost [27].

$$C_{\mathrm{NPC}} = \frac{C_{\mathrm{ann,tot}}}{\mathrm{CRF}(i,N)} \tag{24}$$

where:

- $C_{\mathrm{ann,tot}}$ = total annualized system cost ($/year);
- CRF($i$,$N$) = capital recovery factor;
- $i$ = annual real discount rate, expressed as a decimal; and
- $N$ = project lifetime (years).

The capital recovery factor is defined as [28]:

$$\mathrm{CRF}(i,N) = \frac{i(1+i)^N}{(1+i)^N - 1} \tag{25}$$

where:

The symbols $i$ and $N$ have the same meanings as in Equation (24).

HOMER evaluates candidate configurations using specified resource availability, community demand, component characteristics, dispatch strategies, technical constraints, and

economic assumptions. Feasible configurations are ranked by their calculated NPC within the investigated component ranges. In this study, HOMER provides a cross-platform comparison of system configurations, component capacities, generation and storage requirements, and techno-economic indicators. Equations (23)–(25) summarize its built-in economic formulation and were not independently implemented within MG-OPT. The results support comparative system-level assessment but do not validate the complete four-service thermodynamic model or the MATLAB/Simulink disturbance-response model.

#### 3.3.2. Optimization Scope and Asset Limitations

The number of generation, conversion, and storage assets that can be evaluated within the MG-OPT framework depends on the component models, decision variables, constraints, and computational procedures implemented in MATLAB and Python. Although the framework can be extended to include additional technologies and operating configurations, each additional asset requires an appropriate mathematical representation and integration with the existing energy and material balances. Increasing the number of components may also increase computational complexity. Therefore, the present MG-OPT implementation is not assumed to support an unlimited number of independently optimized assets.

HOMER Pro supports multiple generation, storage, and conversion components within a hybrid energy system. Component sizes can be specified using predefined search-space values, while eligible components can also be sized using HOMER's numerical Optimizer. According to the documentation for the HOMER Pro version used in this study, the numerical Optimizer can size up to four eligible component types simultaneously [29]. Additional components may be included through predefined search-space values, with the corresponding configurations evaluated alongside the optimized variables. Therefore, this optimization limit does not restrict the complete hybrid energy system to four physical assets.

In the present study, the number and types of assets evaluated are determined by the selected system architecture, available component models, resource inputs, operating constraints, and sizing configurations. MG-OPT and HOMER are consequently used to investigate comparable system configurations within their respective modelling capabilities without assuming unrestricted scalability or identical mathematical formulations.

### *3.4. MATLAB/Simulink Integrated Dynamic Model*

The MATLAB/Simulink model represents the operation of the interconnected multi-generation system over time. It combines renewable and dispatchable generation, energy conversion, battery and hydrogen storage, freshwater production, cooling, community electricity demand, and control functions. The battery provides short-term electrical support. The hydrogen pathway connects electrolyzer production and storage with fuel-cell backup generation. Electricity, freshwater, hydrogen production, and cooling outputs are recorded separately to show how changes in shared resources affect each service.

The simulations track generation availability, battery power and state of charge, hydrogen production and inventory, fuel-cell output, and individual service outputs. These trajectories cover the prescribed disturbance and the subsequent observation period. They support the calculation of service coverage, the Integrated Service Performance Score (ISPS), and maximum and cumulative performance loss, as described in Section 2. The Disturbance-Period Performance Preservation Index (DPPI) summarizes performance over the prescribed disturbance window. Service restoration time is reported when every service satisfies the specified baseline coverage criterion for the required duration, subject to numerical tolerance. Sections 3.4.1–3.4.4 describe the component models, storage and service pathways, and control and disturbance-response functions.

The model was implemented in MATLAB and Simulink R2026a (Update 5). MATLAB sets model parameters, runs simulations, and processes time-series outputs. Simulink represents conversion relationships, storage behaviour, operating limits, and control logic through interconnected subsystems. These subsystems use standard blocks, including Gain, Sum, Product, Integrator, Switch, Saturation, and logical operators. From Workspace and To Workspace blocks exchange data with MATLAB, while Dashboard blocks display selected operating variables.

Section 2 presents the reference relationships for PEM electrolysis, fuel-cell generation, multi-effect distillation (MED), and absorption cooling. In the disturbance simulations, hydrogen and freshwater production are calculated from allocated electrical power using the assumed specific electricity consumption for each process. Cooling output is calculated using an aggregate conversion factor. The fuel cell is represented as an aggregate electrical converter, with output limited by rated power and accessible hydrogen inventory. Its hydrogen consumption is included in the storage mass balance.

The simulations evaluate how prescribed changes in generation availability, dispatch, and storage affect service delivery. The component representations omit PEM electrolyzer and fuel-cell startup and shutdown transients, electrochemical polarization, MED heat-exchanger and thermal delays, and absorption-chiller generator and condenser response times. The availability schedule determines when the imposed constraints are removed. The assessment then checks service coverage against the pre-disturbance baseline and evaluates storage replenishment separately. Physical equipment repair times are outside the model's scope.

#### 3.4.1. Renewable Generation, WTE/Biogas, and DC Microgrid

PV, wind, geothermal, and WTE/biogas form the principal generation pathways in the proposed system. PV and wind supply variable renewable electricity, while the geothermal and WTE/biogas pathways provide additional generation under the assumed resource conditions. Site-specific geothermal potential and feedstock availability require separate assessment. The DC microgrid links these generation pathways to battery storage, hydrogen production, power conversion, community electrical demand, and the other service subsystems. Changes in generation availability can therefore affect electricity delivery, hydrogen production, freshwater production, and cooling.

In MATLAB/Simulink, each generation pathway is represented separately using its resource inputs, component characteristics, conversion efficiencies, and operating conditions. The outputs are combined within the electrical network, with conversion losses applied at the relevant interfaces. This arrangement allows prescribed reductions or interruptions to be applied to individual generation pathways. The simulations then track their effects on service coverage, storage use, and backup dispatch during the disturbance and after the scheduled restoration of availability.

#### 3.4.2. Battery and Hydrogen Energy Storage

Battery and hydrogen storage provide complementary electrical support within the multigeneration system. The battery balances short-term differences between generation and demand. The hydrogen pathway uses electricity for PEM electrolysis and stores the produced hydrogen for subsequent fuel-cell generation. The model tracks hydrogen production and stored inventory separately because the fuel cell can continue to draw on stored hydrogen when production falls.

In MATLAB/Simulink, battery dispatch responds to the electrical power balance within the battery's power and state-of-charge (SOC) limits. The stored energy and SOC change as the battery charges and discharges. The hydrogen storage mass balance accounts

for electrolyzer production and fuel-cell consumption, linking the available inventory to electrical backup capability. During generation deficits, the EMS dispatches the battery first. Fuel-cell support then depends on the remaining power request, rated fuel-cell capacity, and accessible hydrogen inventory. Section 4 specifies the battery capacity and initial SOC, PEM and fuel-cell capacities, hydrogen storage capacity, and conversion parameters.

#### 3.4.3. Freshwater, Cooling, and Community Service Models

The model represents freshwater production, cooling, and community electricity supply as distinct service pathways. MED and absorption cooling are the reference technologies for freshwater and cooling provision. In the disturbance simulations, their outputs are calculated from allocated power using the simplified conversion relationships specified in Section 4. Community electricity demand is accounted for separately from the power allocated to hydrogen production, freshwater production, and cooling. Competition for electrical power can therefore cause different levels of degradation across the four services. The simulated interactions reflect electrical power allocation. Assessing competition for shared heat would require a coupled thermal energy balance.

MATLAB/Simulink records freshwater production, cooling output, community electricity supply, and hydrogen production as separate time series. Each output is compared with its corresponding demand to calculate service coverage before the coverage indicators are combined into the Integrated Service Performance Score (ISPS). Retaining the individual trajectories allows the assessment to identify shortfalls in each service and examine how coverage changes after scheduled restoration of subsystem availability. Section 4 specifies the service demands, subsystem capacities, conversion factors, and initial operating conditions.

#### 3.4.4. Energy Management and Disturbance Response Implementation

The energy management system (EMS) coordinates generation, storage, and service allocation as operating conditions change. During an electrical supply deficit, the EMS dispatches the battery first, subject to its power and state-of-charge (SOC) limits. The fuel cell can supply part or all the remaining power request, depending on its rated capacity and the accessible hydrogen inventory. The assessment uses the resulting service coverage and storage trajectories to determine how effectively these resources support service delivery.

Disturbances are implemented in MATLAB/Simulink through prescribed changes in subsystem availability. Each disturbance has a specified onset, duration, magnitude, and schedule for restoring availability. The simulation records generation availability, battery power and SOC, hydrogen production and inventory, fuel-cell output, and the four service outputs throughout the disturbance and subsequent observation period.

These trajectories provide the basis for calculating individual service coverage, the Integrated Service Performance Score (ISPS), and maximum and cumulative performance loss. The Disturbance-Period Performance Preservation Index (DPPI) summarizes performance during the prescribed disturbance window. After the imposed constraints are removed, the assessment checks whether each service reaches at least the specified threshold relative to its baseline coverage for the required duration. Service restoration time is reported when this criterion is satisfied. Storage replenishment is assessed separately. Section 4 reports the simulation settings, initial conditions, and disturbance timing and magnitude used in the case study.

### *3.5. Model Parameters and Modelling Assumptions*

The integrated model uses component parameters, service-performance definitions, operating assumptions, and probabilistic inputs. Component parameters include generation and storage capacities, conversion efficiencies, battery operating limits, and hydrogen pro-

duction and consumption factors. Freshwater and cooling calculations use the conversion relationships specified for each modelling stage. Battery state of charge and stored hydrogen inventory evolve according to their respective balances. The WTE/biogas pathway uses assumptions for organic-waste availability, biogas yield, energy content, and electrical conversion efficiency. Section 4 reports the numerical values, units, and literature sources or modelling basis for the case-study inputs.

Each service-coverage indicator receives a weight of 0.25 in the reference ISPS calculation. These weights give electricity, freshwater, hydrogen production, and cooling equal influence on the aggregate score. The EMS uses a separate dispatch priority to allocate available power. Equal weighting is a study-defined reference choice because stakeholder-derived service preferences are unavailable.

The fault-tree analysis uses assumed event probabilities for conditional screening. Adjustments based on service coverage or storage conditions condition these inputs on the evaluated scenario. Dependence tests examine selected departures from independence, while Monte Carlo analysis propagates the prescribed input probability distributions through the fault-tree calculation. The resulting percentile intervals describe variation under those distributions. Empirical calibration and confidence intervals for actual failure probabilities would require suitable operating records, consistent event definitions, and observation periods.

ETA provides a conceptual framework for organizing possible response pathways. The eight-state framework classifies operating conditions and response phases when the required service indicators and action records are available. Its classifications describe conditions at the evaluated times. Estimating transition rates and equipment repair-time distributions would require additional models and supporting data. Probability inputs, classification criteria, and component parameters are documented separately so that the assumptions underlying each result can be traced.

### *3.6. Simulation and Disturbance-Response Procedures*

The simulation comprises four stages. These are pre-disturbance operation, disturbance onset, operation under the imposed constraints, and assessment after scheduled restoration of subsystem availability. The pre-disturbance period establishes the reference ISPS, $(P_0)$ and the baseline coverage of each service. The disturbance begins at $(t_d)$ and remains active until the scheduled endpoint $(t_b)$. The simulation then continues through the subsequent observation period to assess service coverage and storage conditions.

Throughout the simulation, the model records generation availability, battery power and state of charge, PEM operation, hydrogen production and inventory, fuel-cell output, and individual service outputs. Generation availability records the imposed supply constraints. Battery state of charge and hydrogen inventory show how stored reserves change, while electrolyzer and fuel-cell outputs describe the operation of the hydrogen pathway. The electricity, freshwater, hydrogen-production, and cooling trajectories show how these changes affect service delivery.

Equation (6) converts each service output into a coverage indicator. Equations (7) and (8) combine these indicators into the Integrated Service Performance Score (ISPS). Equations (13) and (15) quantify maximum and cumulative performance loss over the specified assessment interval. Equation (16) gives the Disturbance-Period Performance Preservation Index (DPPI) over the prescribed disturbance window from $(t_d)$ to $(t_b)$. Individual service coverage and critical-service indicators are reported alongside the ISPS to identify shortfalls within the aggregate score.

After subsystem availability is restored according to the prescribed schedule, each service-coverage trajectory is compared with its pre-disturbance baseline. Service restoration

is confirmed when all four services meet their respective baseline thresholds for the required duration. The elapsed time is measured from disturbance onset to the start of the qualifying interval. If the criterion remains unmet, service restoration is reported as unconfirmed within the simulated period.

Electrical power-balance and storage stock–flow checks assess the numerical consistency of the simulations. FTA, dependence sensitivity tests, and Monte Carlo parameter propagation provide conditional screening under the specified probability assumptions. The eight-state descriptive framework classifies operating conditions and response phases when the required service, inventory, reserve, and action records are available.

## 4. Case Study: Gbamu-Gbamu Community

The proposed modelling and disturbance-response assessment framework is applied to Gbamu-Gbamu, Ogun State, Nigeria. Figure 5 shows the Gbamu-Gbamu community and its existing energy infrastructure. The case study evaluates an integrated hybrid multigeneration system supplying electricity, freshwater, hydrogen, and cooling. Published community and resource information provides the basis for the assessment where available. Additional service requirements and operating conditions are identified as study-defined inputs. Following the workflow in Section 3, the assessment combines MG-OPT multigeneration analysis, HOMER cross-platform comparison, and MATLAB/Simulink simulations under prescribed disturbances. This section specifies the system configuration, numerical inputs, simulation settings, disturbance schedule, and probabilistic and economic assumptions. Section 5 presents the technical performance, disturbance-response, probabilistic screening, and economic results.




**Figure 5.** Gbamu-Gbamu Community and Existing Energy Infrastructure, Ogun State, Nigeria.

### *4.1. Case Study System Configuration and Input Parameters*

The rural setting and agricultural activity of Gbamu-Gbamu motivate the assessment of electricity, freshwater, hydrogen, and cooling as interconnected community services. Published information on the community, available resources, and existing energy installation supports the site characterization. The study introduces additional service requirements and technologies to evaluate the expanded multigeneration configuration. Table 3 summarizes the principal case study parameters and distinguishes reported community and existing-system information from study-defined planning inputs and modelling assumptions.

**Table 3.** Gbamu-Gbamu reference characteristics and multigeneration planning requirements.

| Parameter | Value | Data Classification |
|---|---|---|
| Population | ~5000 | Reported community data |
| Households | ~550 households [30] | Reported community data |
| Solar resource | 4.78 kWh/m$^2$/day | Reported site/resource data |
| Existing PV system | 85 kWp | Reported existing system |
| Existing diesel generator | 67 kVA | Reported existing system |
| Reported electricity demand | 338.12 kWh/day | Reported community demand |
| Modelled electricity requirement | 620 kWh/day (25.83 kW average) | Case-study planning input |
| Commissioning year | 2018 | Reported existing-system information |
| Freshwater requirement | 750 m$^3$/day | Case-study planning input |
| Hydrogen requirement | 37.5 kg/day | Case-study planning input |
| Proposed PV and wind capacities | PV: 250 kW; wind: 150 kW | Study-defined baseline sizing |
| Proposed battery and hydrogen storage | Battery: 350 kWh; $H_2$ tank: 300 kg | Study-defined baseline sizing |
| PEM electrolyzer and fuel cell | PEM: 150 kW; fuel cell: 180 kW | Study-defined baseline sizing |
| Geothermal ORC–Kalina pathway | 175 °C reference temperature; 1263 kW reference power | Study-defined MATLAB/HOMER modelling reference |
| MED freshwater production | GOR: 8.87; 5 effects; 5.57 m$^3$/h reference output | Modelled subsystem reference |
| Absorption cooling | COP: 0.60 (range 0.50–0.70) | Modelled subsystem reference |
| WTE/biogas generation | 1125 m$^3$/day biogas; estimated average electrical output: 98.44 kW | Model-derived planning estimate |
| Biogas storage | 562.5 m$^3$ nominal capacity | Study-defined modelling assumption |
| Cooling requirement | 32.5 kW | Case-study planning input |

The planning requirements define the reference demands used to calculate service coverage and assess performance during prescribed disturbances. Electricity, freshwater, hydrogen, and cooling are evaluated together because they share generation, conversion, and storage resources. Freshwater demand includes domestic and irrigation requirements. Hydrogen demand represents the modelled cooking-fuel equivalent and transportation requirements. These service requirements are study-defined planning targets. Simulated supply is compared with each target to calculate service coverage and identify shortfalls.

The additional generation, storage, and conversion technologies form the proposed modelling configuration. The geothermal ORC–Kalina, MED, absorption-cooling, and WTE/biogas parameters are reference conditions or model-derived estimates. Geothermal resource availability at the site requires a separate assessment. The MED and absorption-cooling reference parameters describe the thermal architecture. The disturbance simulations use the simplified power-allocation factors specified separately for that modelling stage.

### *4.2. Case Study Configuration and Parameterization*

The expanded case study applies the multigeneration architecture described in Section 2 to the planning requirements for Gbamu-Gbamu. The proposed configuration comprises 250 kW of PV generation, 150 kW of wind generation, 350 kWh of battery storage, a 150 kW PEM electrolyzer, a 180 kW fuel cell, and 300 kg of hydrogen storage capacity. The wider

assessment also considers geothermal ORC–Kalina generation, MED freshwater production, absorption cooling, and WTE/biogas generation. These technologies provide interconnected pathways for electricity, freshwater, hydrogen, and cooling. Their shared generation and storage resources allow the assessment to examine how operating constraints affect several services simultaneously. Table 3 distinguishes the proposed capacities and modelling assumptions from the reported characteristics of the existing community installation.

The planning requirements in Table 3 provide the reference demands for the service-coverage calculations. The electrical requirement of 620 kWh/day corresponds to an average demand of $D_E = 25.833$ kW. The remaining reference demands are $D_W = 750$ m$^3$/day for freshwater, $D_H = 37.5$ kg/day for hydrogen, and $D_C = 32.5$ kW for cooling. Each simulated service output is compared with its corresponding requirement using Equation (6). The resulting coverage indicators show the extent to which the proposed configuration meets each planning target under the evaluated operating conditions.

$$C_E(t) = \min\left(1, \frac{S_E(t)}{25.833}\right)$$

$$C_W(t) = \min\left(1, \frac{S_W(t)}{750}\right)$$

$$C_H(t) = \min\left(1, \frac{S_H(t)}{37.5}\right)$$

$$C_C(t) = \min\left(1, \frac{S_C(t)}{32.5}\right)$$

where $S_E(t)$, $S_W(t)$, $S_H(t)$, and $S_C(t)$ denote the time-dependent electricity supplied, freshwater produced, hydrogen produced, and cooling delivered by the MATLAB/Simulink model, respectively. Each supply quantity uses the same units as its corresponding demand. Electricity and cooling are expressed in kW, freshwater in m$^3$/day, and hydrogen production in kg/day. The resulting coverage indicators describe how well each service requirement is met during the simulation.

For the case study assessment, each of the four coverage indicators is assigned a weight of 0.25. The ISPS is therefore calculated as:

$$P(t) = 0.25C_E(t) + 0.25C_W(t) + 0.25C_H(t) + 0.25C_C(t)$$

Individual service-coverage trajectories are reported alongside the ISPS to identify shortfalls in each service. The hydrogen production rate, $S_H(t)$, represents PEM electrolyzer output and determines hydrogen-production coverage. Stored hydrogen inventory is tracked separately because the fuel cell can continue to draw on the remaining reserve when hydrogen production falls or stops.

The planning and component-reference models use study-defined efficiencies to represent conversion and auxiliary losses. The adopted values are 98% for the DC bus, 96% for the bidirectional battery converter, 95% for DC/AC conversion, 98% for the hydrogen-compression interface, 55% for fuel-cell conversion, and 95% for both water pumping and the thermal loop. The treatment of inverter and battery-converter losses follows the approach used in the National Renewable Energy Laboratory's System Advisor Model (SAM), which applies component-specific conversion efficiencies [31]. The assumed fuel-cell efficiency is informed by the SOFC electrical-efficiency characteristics described by the U.S. Department of Energy [32]. The remaining efficiencies are preliminary assumptions for the modelled interfaces and auxiliary processes.

The disturbance simulations use separately specified aggregate conversion factors. Battery charging and discharging efficiencies are each 95%. Hydrogen production requires an assumed 52 kWh/kg, and freshwater production requires 2.5 kWh/m$^3$. Cooling output

is calculated by multiplying allocated electrical power by a factor of 0.60. Fuel-cell generation uses an assumed electrical energy yield of 16.5 kWh/kg of hydrogen, subject to rated power and accessible inventory. This yield applies at the disturbance model's electrical output boundary and is documented separately from the 55% efficiency used in the component-reference assessment. Each modelling stage uses its specified conversion parameters. Battery SOC is initialized at 68% and subsequently changes according to the simulated power balance and operating limits. These conversion and storage inputs are documented separately from the event probabilities used in conditional probabilistic screening.

The WTE/biogas assessment assumes an organic-waste generation rate of 0.5 kg/person/day. For the modelled population of 5000, this gives 2500 kg/day of organic waste. The calculation also assumes a biogas yield of 0.45 $m^3$/kg of waste, an energy content of 6.0 kWh/$m^3$, and an electrical conversion efficiency of 35%. The energy-content assumption is informed by the methane-dependent properties of biogas described by the International Energy Agency [33]. The electrical conversion assumption draws on the biomass power-generation characteristics documented by the U.S. Environmental Protection Agency [34].

These inputs provide a preliminary estimate of generation potential. Actual biogas yield depends on feedstock composition, moisture content, and digestion conditions. Site measurements would be required to establish waste availability and achievable biogas production in Gbamu-Gbamu.

Under the adopted assumptions, estimated daily biogas production is:

$$2500 \times 0.45 = 1125 \text{ m}^3/\text{day}$$

The corresponding gross daily energy potential is:

$$1125 \times 6.0 = 6750 \text{ kWh/day}$$

Applying the assumed electrical conversion efficiency of 35% gives 2362.5 kWh/day of electrical energy. Distributing this energy uniformly over 24 h gives an equivalent average electrical output of:

$$P_{\text{WTE}} = \left( \frac{6750 \times 0.35}{24} \right) = 98.44 \text{ kW}$$

The model uses this equivalent average output to represent the WTE/biogas contribution under the assumed uniform generation profile. This contribution supports community electricity supply and affects the power available for hydrogen production, freshwater production, and cooling.

### *4.3. MG-OPT and HOMER Case Study Implementation*

MG-OPT evaluates how generation, conversion, and storage technologies can jointly supply electricity, freshwater, hydrogen, and cooling under the case-study conditions. Using the parameters in Section 4.2, the analysis compares candidate configurations and operating conditions. It records integrated power output, freshwater production, hydrogen production, cooling output, PEM operation, MED performance, and geothermal energy recovery. These component and service outputs show how changes in one technology affect resource use and production across the system.

Parameter studies examine PEM operating conditions, freshwater requirements, geothermal operating temperature, cooling requirements, and electrical operating conditions. Each study evaluates the resulting changes in service production, conversion performance, and resource allocation. These comparisons provide the basis for the technology-sensitivity and cross-service trade-off results presented in Section 5.

HOMER provides a complementary assessment of technical feasibility, component sizing, and system configuration. MATLAB/MG-OPT calculates multigeneration outputs,

conversion efficiencies, and operating conditions. HOMER evaluates whether the corresponding electrical and hydrogen requirements can be supported by the candidate generation, electrolysis, hydrogen storage, battery storage, and power-conversion capacities. This comparison can identify capacity constraints that limit service provision even when the engineering calculations indicate sufficient energy production. The HOMER cases represent the applicable generation pathways, electrical demand, PEM electrolysis, hydrogen demand and storage, battery storage, and AC/DC conversion. MATLAB evaluates freshwater and cooling outputs using the subsystem relationships and service requirements specified in Section 4.2.

The case study applies two sequential workflows and one parallel workflow. In the MATLAB-to-HOMER workflow, MG-OPT operating conditions and the corresponding electrical and hydrogen requirements are transferred to HOMER to assess the capacities and configurations needed to support them. In the HOMER-to-MATLAB workflow, HOMER identifies feasible configurations within the candidate component ranges. Selected configurations are then evaluated in MATLAB to examine component performance and interactions among the four services. In the parallel workflow, MATLAB/MG-OPT and HOMER independently evaluate comparable system conditions. Their outputs are compared for quantities represented consistently in both environments.

The interpretation accounts for differences in dispatch rules, component representations, sizing options, and model boundaries. Section 5.2 reports the resulting feasibility findings, capacity requirements, cross-platform differences, and subsystem constraints.

### *4.4. Matlab/Simulink Dynamic Case Implementation*

The configuration developed through the MG-OPT and HOMER modelling stages was implemented in MATLAB/Simulink to assess generation, storage, dispatch, and service delivery over time. Each simulation covered a 12 h horizon from $t = 0$ to $t = 12$ h using a variable-step solver. The refined simulation used a maximum step size of $5 \times 10^{-5}$ h. Component capacities remained fixed within each run so that the assessment captured changes in operation under the prescribed conditions.

Battery state of charge (SOC) was initialized at 68%. The hydrogen tank had a capacity of 300 kg and an initial inventory of 0 kg. Stored hydrogen subsequently changed through electrolyzer production and fuel-cell consumption. The model used the simulated inventory to determine the hydrogen available for fuel-cell operation, distinguishing installed storage capacity from available hydrogen mass. The service requirements were 25.8333 kW for electricity, 750 $m^3$/day for freshwater, 37.5 kg/day for hydrogen production, and 32.5 kW for cooling.

The preceding MATLAB analyses examined five operating modes, designated Normal, Water Stress, High Agriculture, High Cooling, and Emergency. Further analyses considered technology sensitivities, community applications, service-specific performance objectives, and PEM–SOEC comparisons. These studies characterized component performance and cross-service trade-offs and informed the selection of representative configurations for the time-dependent simulations.

Four representative operating configurations were evaluated in separate MATLAB/Simulink runs. The simulations recorded generation outputs, battery power and SOC, community electricity supply and unmet demand, hydrogen production and inventory, fuel-cell output, freshwater production, and cooling delivery. The four service outputs were converted into coverage indicators using the planning requirements in Table 3. Each indicator was capped at one and assigned a weight of 0.25 in the Integrated Service Performance Score (ISPS). Individual coverage values and critical-service indicators were retained to identify service-specific shortfalls that the aggregate score could conceal.

The Maximum Cooling Coverage configuration, identified as Simulink Case 4, was selected for the detailed compound-disturbance assessment. Its static MG-OPT outputs yield an ISPS of 0.6222, which is reported separately from the pre-disturbance reference calculated from the MATLAB/Simulink trajectories. Comparisons between the modelling stages account for their different dispatch and conversion representations. The simulated trajectories support the calculation of maximum performance loss, cumulative performance loss, and the Disturbance-Period Performance Preservation Index (DPPI). Following scheduled restoration of subsystem availability, service coverage is assessed against the specified baseline criterion. This assessment characterizes the service response to prescribed availability inputs without resolving physical equipment repair or restart dynamics.

Conditional probabilistic screening uses FTA, selected dependence sensitivity tests, and Monte Carlo parameter propagation under the stated probability assumptions. ETA provides a conceptual structure for response pathways, while the eight-state descriptive framework supports classification when the required indicators and action records are available. The 19 additional disturbance scenarios were evaluated through screening calculations and are distinguished from the four MATLAB/Simulink cases, which provide independently simulated service and storage trajectories. Figure 6 summarizes the principal subsystems and their functional connections in a simplified block diagram. Figure 7 shows the corresponding MATLAB/Simulink implementation, including the complete interconnected model and enlarged subsystem views.

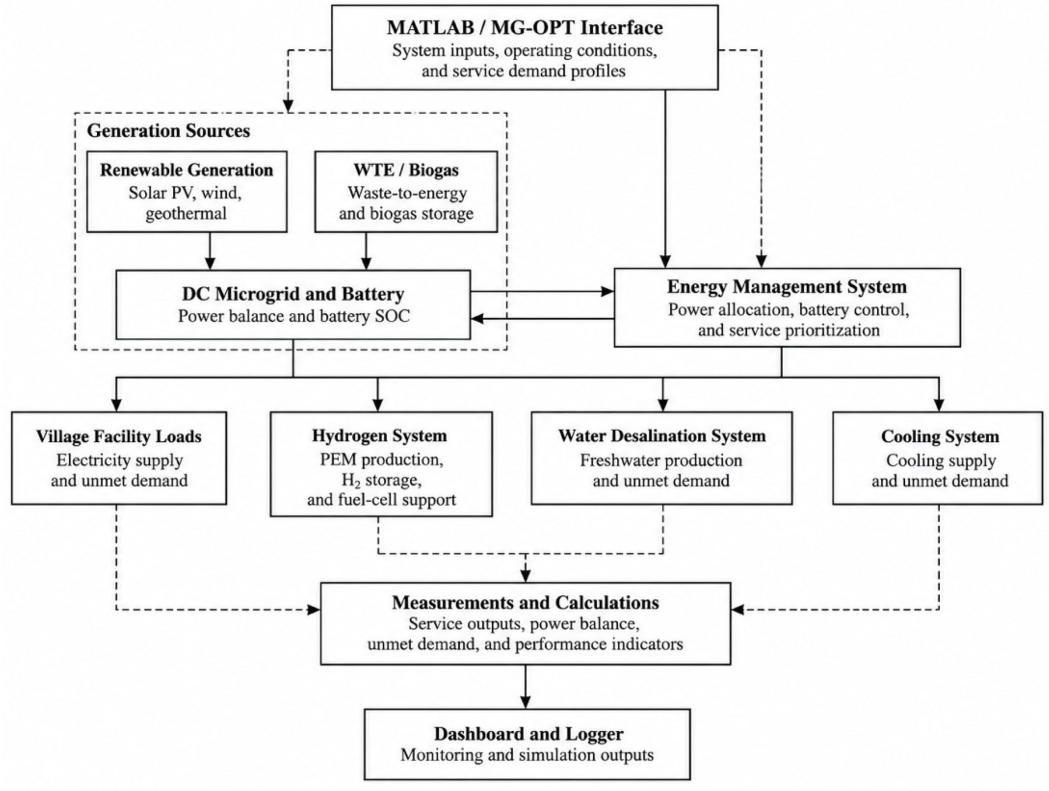


**Figure 6.** Functional block diagram of the integrated MATLAB/Simulink multigeneration model, showing renewable and WTE/biogas generation, the DC microgrid, battery storage, energy management, hydrogen production and storage, freshwater production, cooling, community loads, and connections to the monitoring and control subsystem.

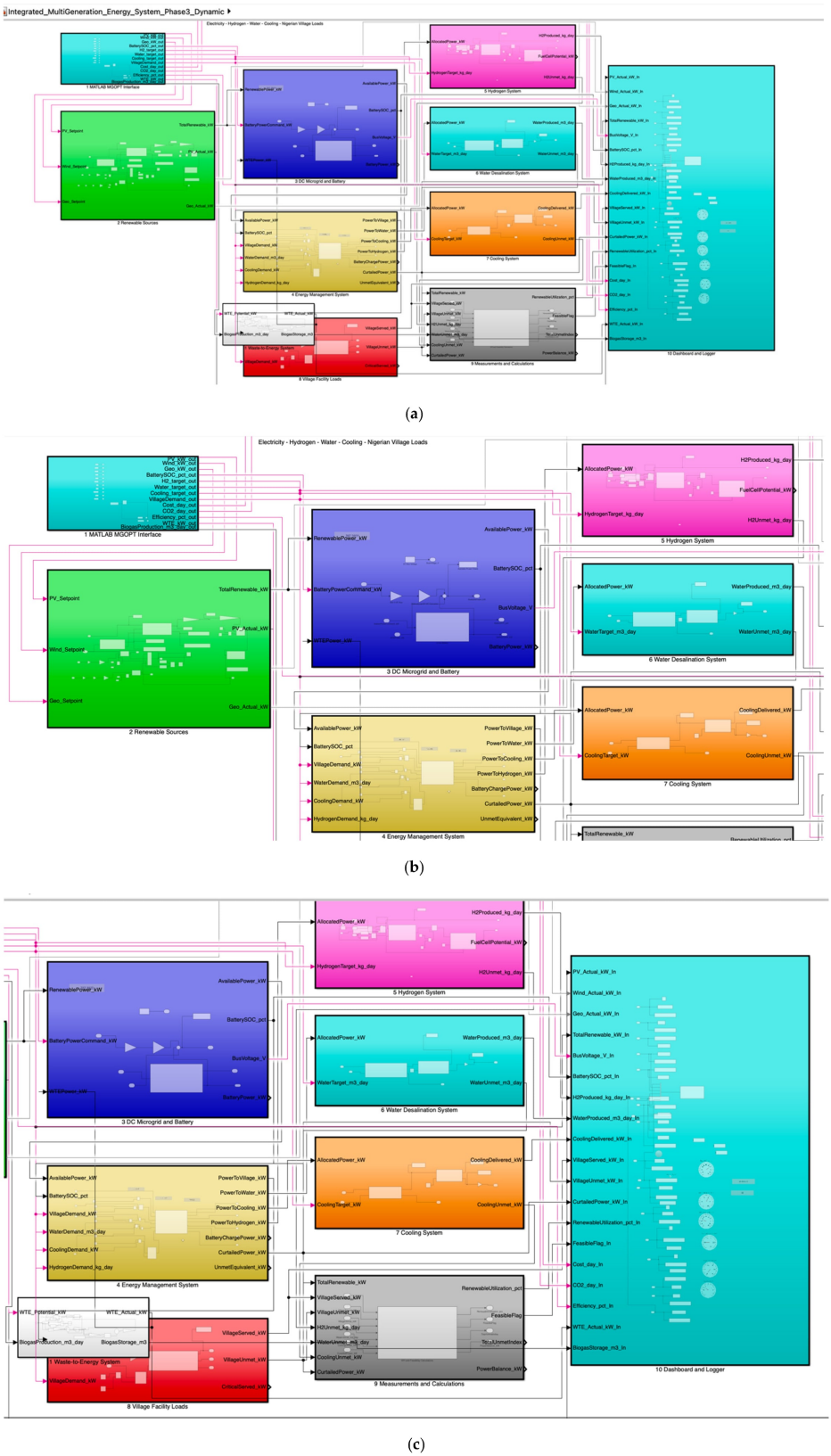


(**a**)

(**b**)

(**c**)

**Figure 7.** MATLAB/Simulink implementation of the integrated multigeneration energy system: (**a**) complete interconnected Simulink model showing the principal subsystems and their connections; (**b**) enlarged view of renewable generation, DC microgrid and battery storage, energy management, hydrogen production, freshwater desalination, and cooling subsystems; and (**c**) enlarged view of WTE/biogas, village facility loads, system measurements and dashboard integration.

### 4.5. Compound Disturbance and Service-Performance Assessment

A compound disturbance is imposed to examine the response of the interconnected renewable-generation, waste-to-energy (WTE)/biogas, and hydrogen-production pathways in the Gbamu-Gbamu case study. Simultaneous reductions in generation availability and electrolyzer availability create constraints that can affect electricity, freshwater, hydrogen production, and cooling. The scenario provides a controlled stress test of the integrated system. Its conditions are study-defined and do not represent a historically observed disturbance or an estimated occurrence frequency for Gbamu-Gbamu.

At the start of the simulation, battery state of charge (SOC) is 68%, hydrogen-storage capacity is 300 kg, and actual stored hydrogen inventory is 0 kg. Battery SOC and hydrogen inventory evolve during the pre-disturbance period, so the reserves available at disturbance onset are determined from the simulated trajectories. Battery dispatch is subject to power and SOC limits, while fuel-cell output is constrained by rated power and accessible hydrogen inventory. Reduced electrolyzer availability can restrict hydrogen replenishment and affect the inventory available for subsequent fuel-cell support. The assessment therefore tracks storage utilization alongside individual service coverage and ISPS.

The study-defined critical-service thresholds are 2.0833 kW for electricity, 75 $m^3$/day for freshwater, and 2 kW for cooling. A separate hydrogen-reserve requirement of approximately 3.0003 kg is also specified. Total village electricity served is compared with the electrical threshold as an aggregate adequacy proxy. Facility-level allocation is not explicitly resolved, so this comparison cannot confirm delivery to individual critical facilities. Hydrogen-reserve adequacy is evaluated using actual stored mass, separately from hydrogen-production coverage. These indicators complement individual service coverage and ISPS by identifying essential-service and reserve shortfalls.

The disturbance begins at approximately 4.001 h, and the affected availability inputs are restored at approximately 8.001 h, giving a prescribed disturbance duration of 4 h. Maximum performance loss, cumulative performance loss, and the Disturbance-Period Performance Preservation Index (DPPI) characterize service degradation over this disturbance window. Simulation continues to 12 h to assess the subsequent service and storage trajectories. Return to baseline service coverage is confirmed only when all four service-coverage indicators satisfy the specified baseline threshold and persistence requirement.

The component models use aggregate conversion relationships and prescribed availability signals. They do not resolve equipment restart delays, electrochemical transients, or thermal response lags. The results therefore describe service degradation and the subsequent response to scheduled restoration of availability inputs. Any reported service restoration time reflects attainment of the specified coverage criterion; it does not establish an independently determined equipment repair time or replenishment of storage reserves. Section 5.4 presents the quantitative findings.

## 5. Results and Analysis

The results progress from multigeneration performance and technology-sensitivity studies to MATLAB–HOMER cross-platform comparison and simulation-based disturbance-response assessment. The analysis examines electricity, freshwater, hydrogen-production, and cooling outputs, together with the trade-offs arising from changes in operating conditions. Deterministic simulations quantify service degradation under prescribed availability constraints and the subsequent response to their scheduled removal. Conditional probabilistic screening and Monte Carlo parameter propagation complement these simulations under the stated probability assumptions. The technology-study operating points are distinguished from the Maximum Cooling Coverage configuration (Simulink Case 4) selected for the detailed disturbance assessment.

### 5.1. MG-OPT Multigeneration Performance and Technology Trade-Offs

Among the investigated technology-study operating points, the absorption refrigeration cooling (ARC) study achieved the highest integrated efficiency, approximately 39.4%. This operating point produced approximately 791.5 kW of total integrated power, 133.7 $m^3$/day of freshwater, 25.24 kg/day of hydrogen, and 200.5 kW of cooling. Its geothermal contribution was approximately 459.7 kW. These results describe the selected technology-study operating point, which differs from the configuration used for the subsequent disturbance assessment.

The highest-efficiency operating point did not satisfy all four planning requirements in Table 3. Freshwater production met approximately 17.8% of the 750 $m^3$/day requirement, while hydrogen production met approximately 67.3% of the 37.5 kg/day requirement. The corresponding shortfalls were approximately 616.3 $m^3$/day of freshwater and 12.26 kg/day of hydrogen. Cooling output exceeded the reference requirement of 32.5 kW, but its coverage indicator remained capped at one. Surplus cooling therefore provided no additional contribution to ISPS beyond full cooling-demand satisfaction and did not eliminate the freshwater or hydrogen shortfalls. These results show that high integrated efficiency does not necessarily indicate adequate provision of every service.

The technology-sensitivity studies used parameter ranges evaluated separately from the fixed component capacities adopted for the disturbance simulations. In particular, the investigated PEM settings were not constrained by the 150 kW electrolyzer rating used in the MATLAB/Simulink case. Increasing the PEM power setting from 220 to 1000 kW increased hydrogen production from approximately 1.98 to 8.28 kg/h. Over the same range, total integrated power decreased from approximately 751 to 478 kW, and integrated efficiency declined from 34.0% to 31.6%. Increasing the freshwater-demand setting from 75 to 350 $m^3$/day increased freshwater production from approximately 3.12 to 14.55 $m^3$/h, while cooling output decreased from approximately 69 to 60 kW. Within the evaluated configurations, these changes demonstrate trade-offs between increased hydrogen or freshwater production and other system outputs.

Increasing the geothermal temperature from 150 °C to 200 °C improved several outputs simultaneously. Total integrated power increased from approximately 746 to 837 kW, hydrogen production from 0.89 to 1.22 kg/h, and cooling output from 52 to 88 kW. Integrated efficiency increased from 32.9% to 35.9%. These results describe the response to the specified geothermal input conditions and do not establish the availability of those conditions at Gbamu-Gbamu.

In the cooling study, increasing the cooling-demand setting from 50 to 500 kW increased delivered cooling from approximately 20 to 200 kW. Total integrated power remained approximately 792 kW, hydrogen production remained approximately 1.05 kg/h, and freshwater production remained approximately 5.57 $m^3$/h. In the electrical/fuel-path study, increasing the power setting from 150 to 1250 kW increased total integrated power from approximately 559 to 1289 kW. Integrated efficiency increased from 31.3% to 38.3%, while hydrogen production increased from approximately 0.90 to 1.48 kg/h.

Table 4 summarizes the investigated input ranges and corresponding changes in service outputs, total integrated power, and integrated efficiency. These sensitivity results show that cross-service interactions depend on the subsystem and operating parameter being varied. Some changes increase one service output while reducing another, whereas others improve several outputs within the investigated model configurations. Individual service outputs and coverage indicators are therefore needed alongside integrated efficiency to assess whether a configuration satisfies the specified community requirements.

**Table 4.** MG-OPT Technology-Sensitivity Results.

| Technology Study | Investigated Input Range | Key Quantitative Response |
| --- | --- | --- |
| PEM electrolysis | Power setting: 220–1000 kW | Hydrogen production: 1.98 → 8.28 kg/h; total integrated power: 751 → 478 kW; integrated efficiency: 34.0% → 31.6% |
| Freshwater/MED | Freshwater-demand setting: 75–350 $m^3$/day | Freshwater production: 3.12 → 14.55 $m^3$/h; cooling output: 69 → 60 kW |
| Geothermal temperature | Temperature: 150–200 °C | Total integrated power: 746 → 837 kW; hydrogen production: 0.89 → 1.22 kg/h; cooling output: 52 → 88 kW; integrated efficiency: 32.9% → 35.9% |
| Cooling | Cooling-demand setting: 50–500 kW | Cooling output: 20 → 200 kW; total integrated power remained approximately 792 kW |
| Electrical/fuel pathway | Power setting: 150–1250 kW | Total integrated power: 559 → 1289 kW; hydrogen production: 0.90 → 1.48 kg/h; integrated efficiency: 31.3% → 38.3% |

Note: The investigated ranges are input settings used in the technology-sensitivity studies. The arrows indicate changes between the corresponding range endpoints. All reported responses are approximate model outputs, rather than independently validated field measurements. These ranges are separate from the fixed component capacities used in the disturbance simulations.

### *5.2. MATLAB-HOMER Cross-Platform Results*

The MATLAB-HOMER comparison identified hydrogen-production and storage capacities as important constraints within the investigated configurations. In the baseline A-series, the geothermal-only and integrated cases were feasible, with HOMER selecting a 3000 kW geothermal generator, a 220 kW PEM electrolyzer, and 1000 kg of hydrogen-storage capacity. The fuel-only case required a 2490 kW generator, a 250 kW converter, and battery storage within the investigated HOMER configuration. These capacities apply to the cross-platform comparison cases and differ from the fixed capacities used in the disturbance simulations. Where battery storage is reported as a number of units, the equivalent energy capacity depends on the capacity of the selected HOMER battery component.

The B-series evaluated demand growth through the MATLAB-to-HOMER workflow. Electrical, hydrogen, and cooling requirements were increased relative to the baseline configuration. Cases B1, B2, and B3 represented demand multipliers of 1.5, 2.5, and 4, respectively. B1 remained feasible, whereas no feasible solutions were identified for B2 or B3 within the investigated component limits and operating constraints. Hydrogen-production and storage requirements were important limiting factors under these higher-demand conditions.

The operating-mode comparison showed a similar limitation. The balanced case specified hydrogen demand of 46 kg/day and cooling demand of 172 kW. It remained feasible with a 3000 kW geothermal generator, a 220 kW PEM electrolyzer, and 1000 kg of hydrogen-storage capacity. The hydrogen-priority case, which specified hydrogen demand of 250 kg/day, was infeasible within the investigated HOMER component ranges and operating constraints.

These results indicate that increasing electricity-generation capacity alone does not necessarily ensure feasibility under higher service demands. Hydrogen-production and storage capacities must also be coordinated with generation capacity and the specified operating requirements. The infeasible outcomes apply to the evaluated search space and modelling assumptions; they do not establish that configurations outside those limits would also be infeasible.

### *5.3. MATLAB Operating, Application, and Performance Results*

The MATLAB analyses produced distinct service-output profiles across the operating-mode, village-application, and performance-objective studies. The results show how specified operating conditions and service priorities affect electricity, freshwater, hydrogen production, and cooling. Table 5 summarizes the calculated outputs and integrated efficiencies. These results describe static operating cases and are evaluated separately from the subsequent MATLAB/Simulink disturbance simulations.

**Table 5.** MATLAB Operating-Mode, Village-Application, and Performance-Goal Results.

| MATLAB Analysis | Case | Power (kW) | $H_2$ (kg/Day) | Water ($m^3$/Day) | Cooling (kW) | Efficiency (%) |
|---|---|---|---|---|---|---|
| **Operating modes** | Normal | 633 | 17.2 | 119.7 | 10 | 32.0 |
| | Water Stress | 792 | 13.2 | 149.6 | 13 | 31.6 |
| | High Agriculture | 961 | 27.9 | 179.6 | 33 | 32.9 |
| | High Cooling | 828 | 15.1 | 149.6 | 48 | 33.9 |
| | Emergency | 263 | 2.8 | 74.8 | 4 | 26.7 |
| **Village Application** | Home | 633 | 7.9 | 119.7 | 6 | 31.2 |
| | School/Clinic/ Market | 263 | 2.1 | 37.4 | 4 | 26.6 |
| | Water/irrigation | 535 | 4.3 | 149.6 | 8 | 27.0 |
| | Food/Agricultural Storage | 450 | 5.3 | 119.7 | 32 | 29.5 |
| | Transportation | 810 | 32.7 | 124.7 | 9 | 32.8 |
| **Performance Goal** | Maximum Electricity | 982 | 14.5 | 179.6 | 11 | 32.0 |
| | Maximum Water | 792 | 9.7 | 149.6 | 13 | 31.4 |
| | Maximum Cooling | 828 | 10.8 | 149.6 | 48 | 33.6 |
| | Maximum $H_2$ | 785 | 55.8 | 124.7 | 10 | 32.8 |
| | Maximum Resilience | 801 | 22.1 | 149.6 | 21 | 32.6 |

Note: Values are approximate outputs from static MATLAB cases. Operating-mode labels, including Normal and Emergency, identify predefined study conditions. These labels are separate from the eight-state descriptive classifications. Performance-objective labels indicate the intended emphasis of each case and do not establish global optimality. "Maximum Resilience Score" is the original label for a static study case. It does not establish an optimized disturbance response or physically modelled recovery capability.

The operating-mode results show substantial differences in production under the configured conditions. High Agriculture produced the largest integrated power output among the five operating modes, approximately 961 kW. It also produced 27.9 kg/day of hydrogen, 179.6 $m^3$/day of freshwater, and 33 kW of cooling, with an integrated efficiency of 32.9%. Emergency operation produced approximately 263 kW of integrated power, 2.8 kg/day of hydrogen, 74.8 $m^3$/day of freshwater, and 4 kW of cooling. Its integrated efficiency was 26.7%. The 698 kW difference in integrated power, accompanied by lower outputs of the other services, demonstrates the sensitivity of system performance to the specified operating conditions.

High Cooling illustrates a different distribution of service outputs. Cooling increased from approximately 10 kW in Normal operation to 48 kW. Integrated power increased from 633 to 828 kW, and integrated efficiency rose from 32.0% to 33.9%. Hydrogen production

decreased from 17.2 to 15.1 kg/day, whereas freshwater production increased from 119.7 to 149.6 $m^3$/day. The cooling-oriented configuration therefore improved several outputs while reducing hydrogen production. These comparisons characterize the production capabilities of the operating modes without establishing that every community planning requirement was satisfied.

The village-application cases also produced distinct output profiles. Transportation had the highest hydrogen production among these cases, approximately 32.7 kg/day, alongside 810 kW of integrated power. Food/Agricultural Storage produced approximately 32 kW of cooling, reflecting the study's emphasis on refrigeration and cold-storage applications. School/Clinic/Market had a smaller production profile, with approximately 263 kW of integrated power, 2.1 kg/day of hydrogen, 37.4 $m^3$/day of freshwater, and 4 kW of cooling. These results demonstrate how the configured system can be assessed for different community applications. Satisfaction of the corresponding service requirements must be evaluated separately using the relevant demands.

The performance-objective cases further illustrate differences in service provision. Maximum Electricity produced approximately 982 kW of integrated power, whereas Maximum Hydrogen produced 55.8 kg/day of hydrogen with 785 kW of integrated power. Maximum Cooling produced approximately 48 kW of cooling and 828 kW of integrated power. The case labelled Maximum Water produced 149.6 $m^3$/day of freshwater and 792 kW of integrated power. Its freshwater output was lower than the 179.6 $m^3$/day obtained in the Maximum Electricity and High Agriculture cases. The label therefore identifies the intended emphasis of the predefined case rather than the highest freshwater output across all evaluated configurations.

The Maximum Resilience Score case produced approximately 801 kW of integrated power, 22.1 kg/day of hydrogen, 149.6 $m^3$/day of freshwater, and 21 kW of cooling. Its integrated efficiency was 32.6%. These static outputs provide an additional comparison of service provision. The case designation alone does not establish superior performance during a disturbance. Such an assessment requires the corresponding time-dependent service and storage trajectories under specified disturbance conditions.

Across the evaluated cases, no single configuration simultaneously achieved the highest integrated power, hydrogen production, freshwater production, and cooling output. Changes in operating conditions and service priorities altered the distribution of outputs across the interconnected system. Individual service outputs and coverage indicators are therefore needed alongside integrated efficiency and ISPS to identify production trade-offs and remaining demand shortfalls.

The SOEC comparison examined the electrical energy required for hydrogen production under the implemented technology assumptions. Specific electricity consumption decreased from approximately 55 kWh/kg for PEM electrolysis to 33 kWh/kg for SOEC and 30.04 kWh/kg for SOEC with heat recovery. Relative to the PEM reference, these values represent reductions of approximately 40.0% and 45.4%, respectively. These reductions apply to electricity consumption, while SOEC operation also requires thermal energy. The 55 kWh/kg PEM reference applies to this technology comparison and is separate from the 52 kWh/kg assumption used in the disturbance simulations.

These model-based results indicate the potential for recoverable thermal energy to reduce the electrical requirement of high-temperature hydrogen production. Assessing the overall energy benefit also requires consideration of the quantity and temperature of the supplied heat. The reported values characterize the adopted technology representations and are not experimentally validated equipment-performance measurements.

*5.4. Multi-Service Disturbance Response and Conditional Probabilistic Screening*

The MATLAB/Simulink assessment examined four representative operating configurations selected from the MATLAB MG-OPT analyses. The simulations provided time-dependent trajectories for electricity, freshwater, hydrogen production, and cooling. The Maximum Cooling Coverage configuration, identified as Simulink Case 4, was selected for the detailed disturbance assessment to support comparison with the corresponding static MG-OPT case. Its static Integrated Service Performance Score (ISPS) was 0.6222, indicating that the configuration did not fully satisfy all four community planning requirements.

In the static assessment, electricity and cooling each achieved a coverage ratio of 1.0000. Freshwater and hydrogen-production coverage were approximately 0.1995 and 0.2893, respectively. These values identify service shortfalls in the selected configuration before the imposed disturbance is considered. The MATLAB/Simulink assessment separately examined how generation and component-availability constraints affected service delivery over time. Hydrogen production and stored inventory were tracked independently to distinguish reduced production from depletion of the hydrogen available for fuel-cell operation.

During the prescribed disturbance interval from 4.001 to 8.001 h, mean coverage was approximately 0.5560 for electricity, 0.1138 for freshwater, 0.0249 for hydrogen production, and 0.5804 for cooling. Equal weighting of the four indicators gave a mean disturbance-period ISPS of 0.3188. These averages summarize coverage over the disturbance window. They differ from instantaneous minimum coverage and from DPPI, which normalizes mean ISPS by the pre-disturbance reference. Figure 8 compares the mean coverage of the four services.

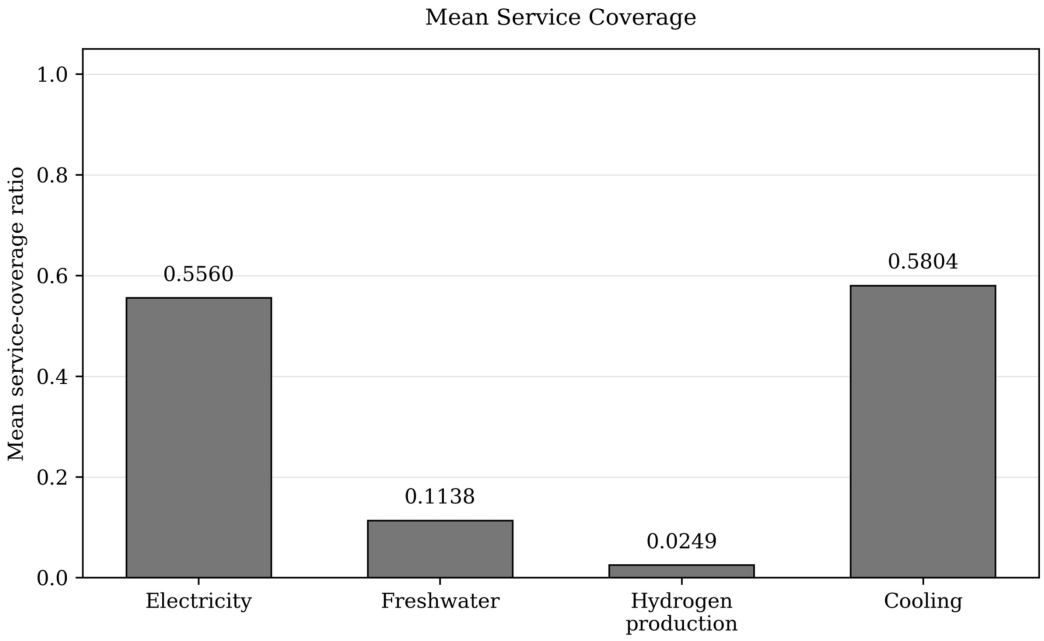


**Figure 8.** Mean service coverage during the prescribed compound disturbance for the Maximum Cooling Coverage configuration, evaluated over 4.001–8.001 h.

Figure 9 shows the time-dependent ISPS trajectory and total village electricity served relative to the critical electrical-load proxy. Together, these plots illustrate the decline in service performance during the prescribed disturbance and the subsequent response to scheduled input restoration. The simulated pre-disturbance reference ISPS was approximately 0.6073, calculated separately from the static MG-OPT value of 0.6222. The minimum disturbance-period ISPS fell approximately to zero. Maximum absolute performance loss was therefore approximately 0.6073, corresponding to a relative loss of approximately

100% at the point of greatest degradation. This instantaneous minimum does not indicate complete service loss throughout the disturbance interval.

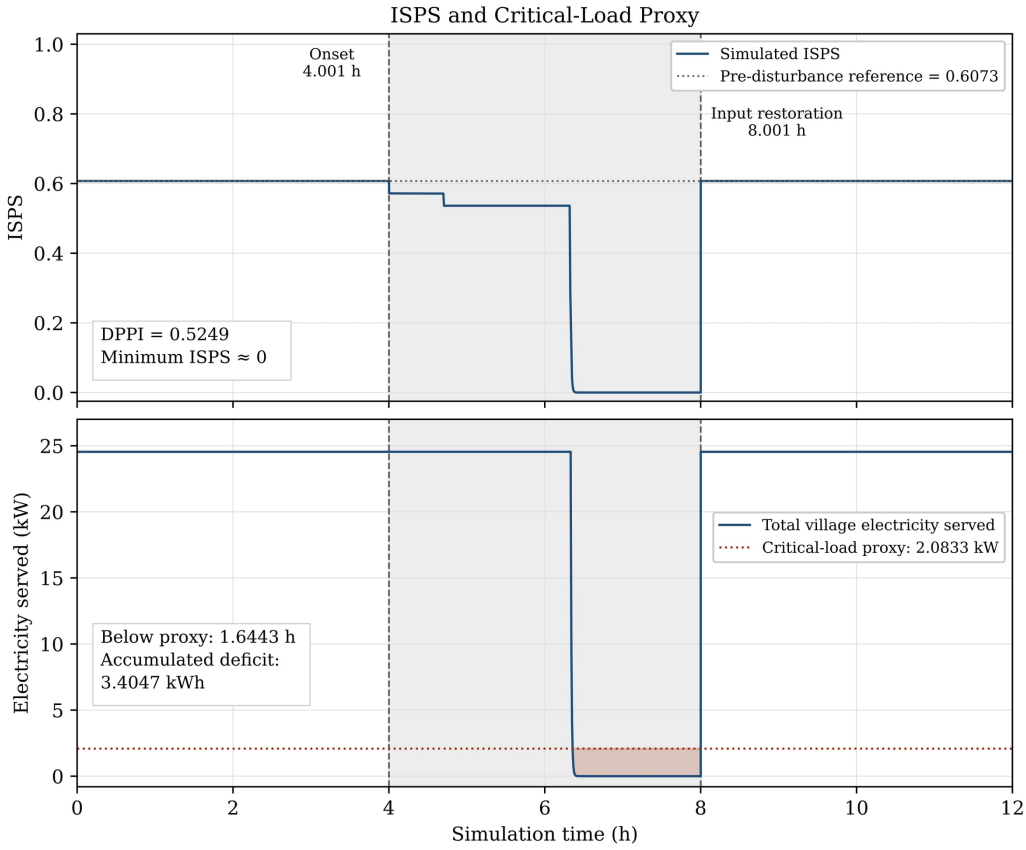


**Figure 9.** Simulated ISPS trajectory and aggregate critical electrical-load proxy assessment, showing disturbance onset at 4.001 h and scheduled input restoration at 8.001 h. The grey shaded region indicates the prescribed disturbance interval from 4.001 to 8.001 h.

Over the 4.001–8.001 h assessment window, cumulative performance loss was 1.1540 ISPS·h, and the Disturbance-Period Performance Preservation Index (DPPI) was 0.5249. Thus, mean ISPS during the disturbance was approximately 52.49% of the simulated pre-disturbance reference. The calculations used the last logged ISPS before disturbance onset as the reference and a left-held integration convention over the specified window. DPPI characterizes performance preservation under the prescribed availability constraints without representing an independent physical restoration process.

Total village electricity served fell below the 2.0833 kW critical electrical-load proxy for approximately 1.6443 h. The accumulated deficit relative to this threshold was 3.4047 kWh. This comparison identifies periods when aggregate electrical supply was insufficient to meet the threshold. It cannot confirm delivery to individual critical facilities because facility-level allocation was not explicitly resolved. Over the complete 12 h simulation, battery discharge supplied approximately 232.7500 kWh, and fuel-cell generation supplied 31.8113 kWh. Electrical power-balance and storage stock–flow checks passed for all four simulated cases. These checks support numerical consistency with the implemented balances rather than validation of detailed equipment behaviour.

Return to baseline service coverage was assessed using a study-defined criterion. Every service-coverage indicator had to reach at least 99% of its respective pre-disturbance value and satisfy the criterion continuously for 15 min. An absolute coverage tolerance floor of $10^{-6}$ was applied. For the selected configuration, the qualifying interval began at 8.001 h

and was confirmed at 8.251 h. The service restoration time, measured from disturbance onset to the start of that interval, was 4.0 h. No additional simulated delay occurred between scheduled input restoration and the start of the qualifying interval.

This result describes a return to baseline coverage following the scheduled removal of availability constraints. It does not establish an independently predicted equipment repair or restart time, or replenishment of storage reserves. Because baseline coverage already included service shortfalls, meeting the restoration criterion did not establish full demand satisfaction. Full satisfaction of all four planned service requirements was not demonstrated within the 12 h simulation horizon. Table 6 summarizes the service-performance and return-to-baseline results for the Maximum Cooling Coverage configuration, including maximum and cumulative performance loss, DPPI, and shortfalls relative to the critical electrical-load proxy. It also reports the prescribed disturbance duration, service restoration time, and persistence requirement used to confirm return to baseline coverage.

**Table 6.** Dynamic service-performance and restoration results for the Maximum Cooling Coverage configuration.

| Performance and Restoration Indicator | Results |
|---|---|
| Simulated Pre-disturbance ISPS, $P_0$ | 0.6073 |
| Minimum disturbance-period ISPS | Approximately 0 |
| Maximum absolute performance loss | 0.6073 |
| Maximum relative performance loss | Approximately 100% |
| Cumulative performance loss, $L_R$ | 1.1540 ISPS·h |
| Disturbance-Period Performance Preservation Index (DPPI) | 0.5249 |
| Mean disturbance-period ISPS | 0.3188 |
| Service restoration time from disturbance onset, $T_R$ | 4.0 h |
| Prescribed disturbance duration | 4.0 h |
| Additional delay to the start of the qualifying interval after input restoration | 0 h |
| Restoration persistence requirement | 15 min |
| Time below the critical electrical-load proxy | 1.6443 h |
| Accumulated critical electrical-load proxy deficit | 3.4047 kWh |
| Full planned-service satisfaction after restoration | Not demonstrated within the simulation horizon |

Note: Performance-loss indicators and DPPI use the 4.001–8.001 h disturbance window. Service restoration time is measured to the start of the qualifying return-to-baseline interval at 8.001 h. The persistence requirement was confirmed at 8.251 h. Return to baseline coverage does not establish full demand satisfaction, reserve replenishment, or physical equipment recovery.

Conditional probabilistic screening was evaluated separately from the simulated service trajectories. Under the original 14-input fault-tree structure and configured scenario-conditioned probabilities, the independent-event top-event probability was 0.250501. Monte Carlo parameter propagation using 2000 samples produced a mean screening probability of 0.250131 and a central 95% parameter-propagation interval of 0.130620–0.403567. Basic-event probabilities were sampled independently from beta distributions centred on the configured values, with a concentration parameter of 30. The interval describes variation under these prescribed parameter distributions. It is not an empirical confidence interval for the actual system-failure probability at Gbamu-Gbamu. Similarly, agreement

between the independent-event calculation and the Monte Carlo mean does not establish field calibration.

The selected dependence tests showed that the screening probability varied with the assumed joint-event distributions. For the original 14-input structure, positive dependence was introduced for two pairs: low photovoltaic output with low wind output, and battery unavailability with fuel-cell unavailability. Applying dependence to both pairs increased the top-event probability from 0.250501 under independence to 0.26669, 0.28276, and 0.31453 at mixture weights of 0.25, 0.50, and 1.00, respectively. The strongest tested setting increased the probability by approximately 6.40 percentage points while preserving the marginal probability of each event. These weights are prescribed sensitivity parameters rather than measured correlation coefficients. The tests address selected dependencies and do not constitute a comprehensive common-cause failure assessment.

A separate structural review excluded storage depletion, cascading failure, and multi-service stress as independent basic-event inputs because these conditions can arise from interactions within the system. Their consequences were examined through the simulated service and storage trajectories. Under the resulting 11-input structure, the independent-event screening probability was 0.104407. Applying dependence to both selected event pairs increased this probability to 0.123754, 0.142954, and 0.180916 at mixture weights of 0.25, 0.50, and 1.00, respectively.

The lower independent-event result for the 11-input structure reflects the removal of three inputs and their associated Boolean contributions. It does not demonstrate an improvement in physical system performance. Both structures produce conditional screening results that depend on the retained event definitions, assumed probabilities, and dependence settings. Neither establishes an empirically calibrated causal failure model. ISPS and service restoration time are calculated separately from deterministic simulation trajectories. For reference, Table 7 summarizes the original 14-input baseline, including the independent-event FTA probability, Monte Carlo sample size, beta-distribution concentration parameter, and resulting mean and central 95% parameter-propagation interval. These results describe screening outcomes under the stated assumptions. Figure 10 compares the independent-event FTA screening probability with the Monte Carlo mean and central 95% parameter-propagation interval for the original 14-input baseline. The plot shows the close agreement between the two central estimates and the spread of screening results arising from the assumed probability distributions. This agreement does not establish field calibration.

**Table 7.** Conditional FTA and Monte Carlo parameter-propagation results for the original 14-input baseline.

| Probability/Uncertainty Indicator | Results |
|---|---|
| Independent-event FTA top-event probability | 0.250501 |
| Monte Carlo samples | 2000 |
| Beta distribution concentration parameter | 30 |
| Mean Monte Carlo top-event probability | 0.250131 |
| Central 95% parameter-propagation interval | 0.130620–0.403567 |

The probabilistic screening does not generate service trajectories or restoration times from sampled barrier outcomes or state-transition rates. ETA provides a conceptual structure for response pathways. The eight-state descriptive framework supports classification when the required service, inventory, reserve, and operational-action information is available. Changes in service output alone do not establish that emergency actions or repair activities occurred. Assignment of the Recovered state also requires explicit confirmation of the specified service and response criteria.

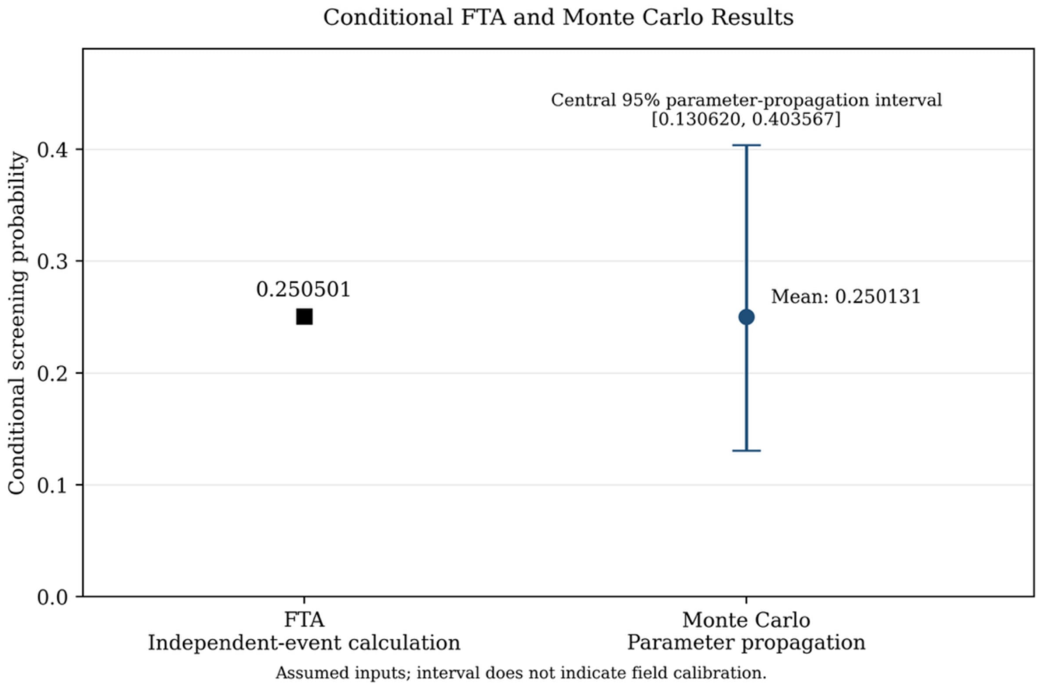


**Figure 10.** Independent-event FTA screening probability and Monte Carlo parameter-propagation results for the original 14-input baseline. The interval represents variation under the assumed parameter distributions and does not indicate field calibration.

The combined results support retaining individual service trajectories alongside ISPS, storage utilization, and critical-service indicators. The implemented inventory and dispatch constraints capture changes in backup support as stored energy is used. However, the models do not resolve hydrogen pressure–temperature coupling, minimum delivery pressure, fuel-cell warm-up, MED fouling and thermal delays, biogas-yield variability, or absorption-chiller part-load dynamics. The simulated response to scheduled input restoration therefore remains conditional on prescribed availability signals and aggregate conversion relationships. Detailed component models and supporting operating data would be required to predict physical equipment recovery.

### *5.5. Techno-Economic Results and Sensitivity*

The lifecycle techno-economic assessment estimated an initial capital cost of approximately USD 7.887 million, annual operating expenditure of USD 298,052, and a net present cost (NPC) of USD 11.703 million. The corresponding levelized costs were USD 1.015/kWh for electricity (LCOE), USD 5.394/$m^3$ for freshwater (LCOW), USD 28.26/kg for hydrogen (LCOH), and USD 0.817/kWh of delivered cooling (LCOC). These estimates include dedicated equipment costs and allocated shares of common system costs. They describe the evaluated multigeneration configuration under the adopted cost, operating, and financing assumptions.

The sensitivity analysis identified capital investment and discount rate as important influences on NPC. Reducing capital cost by 25% decreased NPC from USD 11.703 million to USD 9.193 million. Increasing capital cost by 25% raised NPC to $14.212 million, giving a range of approximately USD 5.02 million between the two sensitivity cases. Increasing the real discount rate from 4% to 12% reduced NPC from approximately USD 12.924 million to USD 10.383 million. This reduction reflects the lower present value assigned to future expenditure at higher discount rates.

Variation in anaerobic-digestion (AD) cost produced a narrower NPC range of USD 11.516–USD 11.889 million. Within the investigated sensitivity ranges, overall capital cost and discount-rate assumptions therefore had a greater effect on NPC than AD cost. This comparison applies to the parameter ranges tested and does not establish their relative influence under all possible conditions.

The integrated system supplies four services, requiring shared lifecycle costs to be allocated among electricity, freshwater, hydrogen, and cooling. Each levelized cost consequently depends on the adopted allocation method and the service quantities used in its calculation. The reported values are preliminary model-based estimates for the specified configuration and assumptions. They should be interpreted alongside service provision and capacity constraints when assessing the economic implications of the proposed system.

## 6. Conclusions

This study developed an integrated modelling framework to evaluate technical performance, multi-service disturbance response, and lifecycle economics for a proposed rural multigeneration system supplying electricity, freshwater, hydrogen, and cooling. MG-OPT, HOMER, and MATLAB/Simulink were used to examine technology interactions, operating conditions, cross-service trade-offs, and system feasibility. The technology studies showed that higher integrated efficiency does not necessarily ensure satisfaction of every service requirement. The cross-platform comparison identified capacity constraints within the investigated configurations, demonstrating the need to coordinate generation, storage, conversion, and service requirements.

Four representative configurations were evaluated through MATLAB/Simulink simulations. The Maximum Cooling Coverage configuration was selected for the detailed compound-disturbance assessment. Its simulated ISPS decreased from a pre-disturbance reference of 0.6073 to approximately zero at the minimum recorded point, corresponding to a maximum relative performance loss of approximately 100%. This instantaneous minimum did not represent complete service loss throughout the disturbance. Over the prescribed 4-hour disturbance window, cumulative performance loss was 1.1540 ISPS·h, and the Disturbance-Period Performance Preservation Index (DPPI) was 0.5249. The latter indicates that mean ISPS during the disturbance was approximately 52.49% of its pre-disturbance reference.

The qualifying return-to-baseline interval began at 8.001 h and was confirmed at 8.251 h. Each service had to maintain at least 99% of its respective baseline coverage for 15 min, with an absolute coverage tolerance floor of $10^{-6}$. The resulting service restoration time from disturbance onset was 4.0 h. Return to baseline coincided with scheduled removal of the availability constraints and did not establish an independently predicted equipment repair or restart time. Full satisfaction of all planned service requirements was not demonstrated within the simulation horizon because the baseline itself contained service shortfalls.

Conditional probabilistic screening was evaluated separately from the simulated service trajectories. The original 14-input fault tree produced an independent-event top-event probability of 0.250501. Monte Carlo parameter propagation yielded a mean of 0.250131 and a central 95% parameter-propagation interval of 0.130620–0.403567. The strongest tested positive dependence for both selected event pairs increased the screening probability to 0.31453. The separate 11-input structural review produced an independent-event probability of 0.104407, increasing to 0.180916 under the strongest corresponding dependence setting. These differences reflect changes in tree structure and joint-event assumptions rather than demonstrated improvements or deterioration in physical system performance. The results remain conditional on assumed probability inputs and do not establish field-calibrated failure frequencies.

The eight-state descriptive framework provides classifications when the required service, inventory, reserve, and operational-action information is available. ETA organizes possible response pathways conceptually. Neither approach establishes equipment repair-time distributions or independently predicts physical recovery. The economic assessment estimated an NPC of approximately USD 11.703 million under the adopted assumptions. Capital investment and discount rate substantially influenced NPC within the tested sensitivity ranges, while shared-cost allocation affected the interpretation of individual service costs.

For the Gbamu-Gbamu planning case, the framework supports examination of service interdependencies, capacity constraints, and performance preservation under prescribed disturbances. Its present scope is limited by aggregate conversion relationships and the absence of suitable site-specific reliability and restoration records. The disturbance model does not resolve detailed electrochemical and thermal transients, hydrogen pressure–temperature effects, variable biogas production, MED fouling, or absorption-chiller part-load behaviour. Numerical conservation checks support consistency with the implemented balances but do not validate these omitted processes. Future development requires component-specific dynamic models, evidence-supported probability inputs, and comparison with observed operating behaviour before the framework can predict physical equipment recovery.

**Author Contributions:** Conceptualization, Z.L. and H.A.G.; methodology, Z.L. and H.A.G.; software Z.L.; validation Z.L. and H.A.G.; formal analysis, Z.L. and H.A.G.; investigation, H.A.G.; data curation, Z.L.; writing—original draft preparation, Z.L.; writing—review and editing, Z.L. and H.A.G.; visualization, Z.L.; supervision, H.A.G.; project administration, H.A.G. All authors have read and agreed to the published version of the manuscript.

**Funding:** This research was funded by NSERC, grant number 210503.

**Data Availability Statement:** Data sets are produced for this paper. Data is available upon request.

**Acknowledgments:** Thank you to the members of the Smart Energy System Laboratory at Ontario Tech University for their valuable support to this research. This research was supported and funded by the Natural Sciences and Engineering Research Council of Canada (NSERC).

**Conflicts of Interest:** The authors declare no conflicts of interest.

## Abbreviations

The following abbreviations are used in this manuscript:

| | |
|---|---|
| HES | Hybrid Energy System |
| EMS | Energy Management System |
| MG-OPT | Multi-Generation Optimization Framework |
| PV | Photovoltaic |
| SOFC | Solid Oxide Fuel Cell |
| PEM | Proton Exchange Membrane Electrolyzer |
| MED | Multi-Effect Distillation |
| $H_2$ | Hydrogen |
| RES | Renewable Energy Sources |
| BESS | Battery Energy Storage System |
| LLM | Large Language Model |
| KPI | Key Performance Indicator |
| SOC | State of Charge |
| HOMER | Hybrid Optimization of Multiple Energy Resources |
| ARC | Absorption Refrigeration Cycle |
| GT | Gas Turbine |
| RE-LLaMA | Renewable Energy Large Language Model |
| ORC | Organic Rankine Cycle |
| MPPT | Maximum Power Point Tracking |

| | |
|---|---|
| FTA | Fault Tree Analysis |
| COP | Coefficient of Performance |
| ISPS | Integrated Service Performance Score |
| MC | Monte Carlo |
| WTE | Waste-to-Energy |
| AD | Anaerobic Digestion |
| NPC | Net Present Cost |
| LCOE | Levelized Cost of Electricity |
| LCOH | Levelized Cost of Hydrogen |
| GOR | Gained Output Ratio |
| LCOC | Levelized Cost of Cooling |
| DC | Direct Current |
| LCOW | Levelized Cost of Water |
| AC | Alternating Current |
| LPSP | Loss of Power Supply Probability |
| DPPI | Disturbance-Period Performance Preservation Index |
| ETA | Event Tree Analysis |

## References


1. IRENA; KfW; GIZ. The Renewable Energy Transition in Africa: Powering Access, Resilience and Prosperity. 2021. Available online: https://www.irena.org/-/media/Files/IRENA/Agency/Publication/2021/March/Renewable_Energy_Transition_Africa_2021.pdf (accessed on 4 November 2026).
2. IRENA. Sub-Saharan Africa: Policies and Finance for Renewable Energy Deployment. 2024. Available online: https://www.irena.org/-/media/Files/IRENA/Agency/Publication/2024/Jul/IRENA_SS_Africa_policies_finance_RE_2024.pdf (accessed on 4 November 2026).
3. Ahmadi, S.; Gharehghani, A.; Soltani, M.M.; Fakhari, A.H. Design and evaluation of renewable energies-based multi-generation system for hydrogen production, freshwater and cooling. *Renew. Energy* **2022**, *198*, 916–935. [CrossRef]
4. Alirahmi, S.M.; Rostami, M.; Hamzeh Farajollahi, A. Multi-criteria design optimization and thermodynamic analysis of a novel multi-generation energy system for hydrogen, cooling, heating, power, and freshwater. *Int. J. Hydrogen Energy* **2020**, *45*, 15047–15062. [CrossRef]
5. Chitgar, N.; Emadi, M.A. Development and exergoeconomic evaluation of a SOFC-GT driven multi-generation system to supply residential demands: Electricity, fresh water and hydrogen. *Int. J. Hydrogen Energy* **2021**, *46*, 17932–17954. [CrossRef]
6. Yapicioglu, A.; Dincer, I. A newly developed renewable energy driven multigeneration system with hot silica sand storage for power, hydrogen, freshwater and cooling production. *Sustain. Energy Technol. Assess.* **2023**, *55*, 102938. [CrossRef]
7. Zheng, S.; Wu, Z.; Zhou, X. Economic and environmental analysis of a new sustainable multi-generation system for power, heating, cooling, freshwater, and hydrogen production. *Energy* **2025**, *328*, 136465. [CrossRef]
8. Simpson, G.B.; Jewitt, G.P.W.; Becker, W.; Badenhorst, J.; Masia, S.; Neves, A.R.; Rovira, P.; Pascual, V. The water-energy-food nexus index: A tool to support integrated resource planning, management and security. *Front. Water* **2022**, *4*, 825854. [CrossRef]
9. Ahmed, F.E.; Hashaikeh, R.; Hilal, N. Hybrid technologies: The future of energy efficient desalination—A review. *Desalination* **2020**, *495*, 114659. [CrossRef]
10. Ghaffour, N.; Bundschuh, J.; Mahmoudi, H.; Goosen, M.F.A. Renewable energy-driven desalination technologies: A comprehensive review on challenges and potential applications of integrated systems. *Desalination* **2015**, *356*, 94–114. [CrossRef]
11. O'Dwyer, E.; Pan, I.; Charlesworth, R.; Butler, S.; Shah, N. Integration of an energy management tool and digital twin for coordination and control of multi-vector smart energy systems. *Sustain. Cities Soc.* **2020**, *62*, 102412. [CrossRef]
12. Gabbar, H.A. Resiliency analysis of hybrid energy systems within interconnected infrastructures. *Energies* **2021**, *14*, 7499. [CrossRef]
13. Hosseini, S.; Barker, K.; Ramirez-Marquez, J.E. A review of definitions and measures of system resilience. *Reliab. Eng. Syst. Saf.* **2016**, *145*, 47–61. [CrossRef]
14. Poulin, C.; Kane, M. Infrastructure resilience curves: Performance measures and summary metrics. *Reliab. Eng. Syst. Saf.* **2021**, *216*, 107926. [CrossRef]
15. Tong, W.; Li, H.X.; Nasirzadeh, F.; Ji, Y.; Yao, F.; Zhou, R. Resilience performance analysis of interdependent infrastructures using fault tree and dynamic Bayesian network. *Reliab. Eng. Syst. Saf.* **2026**, *272*, 112541. [CrossRef]
16. Zeng, Z.; Fang, Y.-P.; Zhai, Q.; Du, S. A Markov reward process-based framework for resilience analysis of multistate energy systems under the threat of extreme events. *Reliab. Eng. Syst. Saf.* **2021**, *209*, 107443. [CrossRef]
17. International Energy Agency (IEA). Financing Electricity Access in Africa—State of Play. 2025. Available online: https://www.iea.org/reports/financing-electricity-access-in-africa/state-of-play (accessed on 4 November 2026).

18. World Bank. Electricity Trade to Unlock Affordable and Reliable Electricity in West Africa. 2020. Available online: https://www.worldbank.org/en/news/press-release/2020/07/28/electricity-trade-to-unlock-affordable-and-reliable-electricity-in-west-africa (accessed on 4 November 2026).
19. World Bank. The World Bank Approves Additional Financing to Consolidate the Gains of Nigeria's Power Sector Recovery Program. 2023. Available online: https://www.worldbank.org/en/news/press-release/2023/06/09/the-world-bank-approves-additional-financing-to-consolidate-the-gains-of-nigeria-s-power-sector-recovery-program (accessed on 4 November 2026).
20. Babalola, S.O.; Daramola, M.O.; Iwarere, S.A. Socio-economic impacts of energy access through off-grid systems in rural communities: A case study of Southwest Nigeria. *Philos. Trans. R. Soc. A* **2022**, *380*, 20210140. [CrossRef] [PubMed]
21. Bastien, R.; Feng, M.; Liebe, U. Towards equitable, integrated, and adaptive water-energy-food nexus research in Africa: A systematic literature review. *Environ. Impact Assess. Rev.* **2025**, *115*, 108043. [CrossRef]
22. Botai, J.O.; Botai, C.M.; Ncongwane, K.P.; Mpandeli, S.; Nhamo, L.; Masinde, M.; Adeola, A.M.; Mengistu, M.G.; Tazvinga, H.; Murambadoro, M.D.; et al. A review of the water–energy–food nexus research in Africa. *Sustainability* **2021**, *13*, 1762. [CrossRef]
23. Ursua, A.; Gandia, L.M.; Sanchis, P. Hydrogen production from water electrolysis: Current status and future trends. *Proc. IEEE* **2012**, *100*, 410–426. [CrossRef]
24. Prajapati, M.; Shah, M.; Soni, B. A comprehensive review of the geothermal integrated multi-effect distillation (MED) desalination and its advancements. *Groundw. Sustain. Dev.* **2022**, *19*, 100808. [CrossRef]
25. Gabbar, H.A.; Hemied, O.S. MG-OPT: Intelligent multi-objective Pareto-based optimization framework and transactive energy for hybrid renewable energy systems with hydrogen integration. *Energy Convers. Manag.* **2025**, *341*, 120042. [CrossRef]
26. HOMER Energy. Welcome to HOMER. HOMER Pro Documentation. Available online: https://homerenergy.com/products/pro/docs/latest/index.html (accessed on 4 November 2026).
27. HOMER Energy. Total Annualized Cost. HOMER Pro Documentation. Available online: https://homerenergy.com/products/pro/docs/latest/total_annualized_cost.html (accessed on 4 November 2026).
28. HOMER Energy. Capital Recovery Factor. HOMER Pro Documentation. Available online: https://homerenergy.com/products/pro/docs/latest/capital_recovery_factor.html (accessed on 4 November 2026).
29. HOMER Energy. Optimization. HOMER Pro Documentation. Available online: https://homerenergy.com/products/pro/docs/latest/optimization.html (accessed on 4 November 2026).
30. Elegeonye, H.I.; Owolabi, A.B.; Ohunakin, O.S.; Yakub, A.O.; Yahaya, A.; Same, N.N.; Suh, D.; Huh, J.-S. Techno-economic optimization of mini-grid systems in Nigeria: A case study of a PV–battery–diesel hybrid system. *Energies* **2023**, *16*, 4645. [CrossRef]
31. National Renewable Energy Laboratory (NREL). Battery Storage: Behind the Meter. System Advisor Model (SAM) Documentation. Available online: https://samrepo.nlr.gov/help/battery_storage_btm.html (accessed on 4 November 2026).
32. U.S. Department of Energy. Comparison of Fuel Cell Technologies. Available online: https://www.energy.gov/cmei/fuels/comparison-fuel-cell-technologies (accessed on 4 November 2026).
33. International Energy Agency (IEA). Outlook for Biogas and Biomethane: Introduction to Biogas and Biomethane. 2025. Available online: https://www.iea.org/reports/outlook-for-biogas-and-biomethane/introduction-to-biogas-and-biomethane-2 (accessed on 4 November 2026).
34. U.S. Environmental Protection Agency (EPA). Biomass Combined Heat and Power Catalog of Technologies (Version 1.1). 2007. Available online: https://www.epa.gov/sites/default/files/2015-07/documents/biomass_combined_heat_and_power_catalog_of_technologies_v.1.1.pdf (accessed on 4 November 2026).


**Disclaimer/Publisher's Note:** The statements, opinions and data contained in all publications are solely those of the individual author(s) and contributor(s) and not of MDPI and/or the editor(s). MDPI and/or the editor(s) disclaim responsibility for any injury to people or property resulting from any ideas, methods, instructions or products referred to in the content.